

Discrete Continuum Robotic Structures

by

Alfonso Parra Rubio

B.A Aerospace Engineering, UEM (2016)

Submitted to the Media Arts and Sciences, School of Architecture and
Planning

in partial fulfillment of the requirements for the degree of

Master of Science

at the

MASSACHUSETTS INSTITUTE OF TECHNOLOGY

August 2020

© Massachusetts Institute of Technology 2020. All rights reserved.

Author
Media Arts and Sciences, School of Architecture and Planning
August 2021

Certified by
Neil Gershenfeld
MIT Professor and Director of the Center for Bits and Atoms
Thesis Supervisor

Accepted by
Tod Machover
Academic Head, Program in Media Arts and Sciences

Discrete Continuum Robotic Structures

by

Alfonso Parra Rubio

Submitted to the Media Arts and Sciences, School of Architecture and Planning
on August 2021, in partial fulfillment of the
requirements for the degree of
Master of Science

Abstract

When overcoming environmental constraints, nature shows the capacity to generate hybrid hard-soft morphing continuum structures at very low cost at almost any scale. Human attempts to replicate nature-like systems to overcome modern engineered solutions, based on classical rigid mechanics, commonly lead to hyper-redundant and complicated designs. Novel trends like soft robotics or continuum robotics are showing new successful directions but mostly at small sizes. It is still a challenge to achieve accessible and cost-efficient scalable nature-like solutions.

The earliest research towards digital materials focused on proving reversibility of their assembly, their low relative densities vs. ultra-high stiffness ratios and scalability properties. Now we can find architected metamaterials with many kinds of exotic physical properties. This thesis will focus on digital materials with custom mechanical properties. Recent work showed the capacity to generate controlled mechanical anisotropies as embedded compliancy, chirality, and auxeticity. That enables generating continuum macroscopic foams with controlled deformation that could preserve some properties and help bring simplicity to overcome tasks that, with classic rigid-joint mechanical systems, would require a very complex system.

Equally important, many of the modern engineering solutions that would require digital materials are very dependent on their outer shape. Literature shows less acclaim for providing an accurate shape to these digital materials. Some of the strategies proposed have been based on hierarchical strategies or reducing the overall size of the building blocks but these findings conflict with the many of the claimed premises. This thesis is proposing a folded solution that will integrate onto the continuum structure and provide a desired shape that is structurally efficient while respecting its intrinsic degrees of freedom.

As a whole, this thesis explores if heterogeneous digital materials can provide all the mechanical needs of a movable structure integrated. This thesis tries to mimic nature's engineering strategies by joining the kinematical and shape-form needs into a single material system composed of a discrete building block core and a folded outer-mold-line layer. As examples, this thesis recreates a water snake and a morphing wing inspired by birds camber morphing.

Thesis Supervisor: Neil Gershenfeld

Title: MIT Professor and Director of the Center for Bits and Atoms

Acknowledgments

The real path to anywhere is the people you interact with. Thus, I need to thank a lot of them:

I would like to sincerely say thank you to Neil Gershenfeld. Thanks for bringing me here, open the door to this amazing place as MIT is, and letting me be a member of the CBA family.

To the CBA folks and MIT friends. The biggest surprise at MIT has been the people. You are such giving beings and I will be always in debt to you. From the past generation (Sam, Ben, Joao, Filippou, Will..) that served as reference roles and showed me which errors I should avoid in this particular place, to the contemporaneous group (Dixia, Camron, Zach, Dave, Eyal, Patricia, Amira, Jake, Erik, Jack, Justin, Christopher) that navigated with me when I committed one by one those errors I was told. Your talent is out of the scope.

Thank you CBA to be a shelter in so many ways for me when a global pandemic was hitting homogeneously all over the world. Thanks to the CBA staff to protect us and care for us.

Muchísimas gracias a mi familia por apoyarme en cada decisión que he tomado, por hacerme las preguntas adecuadas en los momentos adecuados que más que preguntas, eran deberes para reflexionar. Por entender que a pesar de estar en el siglo de la revolución tecnológica personal, la distancia siempre va a ser tangible y muy difícil de quitar de la ecuación. Por estar sin estar. Por querer sin poder tocar.

No podría estar más orgulloso de mis amigos de Baza con los que crecí, y de mis amigos de Madrid con los que florecí. Gracias por mantener mis inquietudes siempre alerta y mi corazón contento. Pbar se cuece.

Thanks a lot to the people that two years ago, in my early days here, grabbed my hand, welcomed me here, and told me that this is now the place I belong. Heather, Arber, and many 3rds, you are such unique human beings.

And last but not least, thanks to the people that made this new city became home. To Cam to invite me to make a home in Church St with two lovely felines, to The

Cube people, Das House people, Spanish Mafia people, and many random human beings I've met here. You build for me a freak mattress of comfort and constant curiosity that literally, keeps me going.

Discrete Continuum Robotic Structures

by

Alfonso Parra Rubio

This thesis has been reviewed and approved by the following committee members:

Professor Neil Gershenfeld

MIT Professor
Director at the MIT Center for Bits and Atoms

Professor Dixia Fan

MIT Sea Grant
Queen's University Professor

Professor Skylar Tibbits

MIT Professor
Co-Director of the Self Assembly Lab.

Contents

1	Introduction	11
2	Lattice and Actuation	19
2.1	Mechanical Anisotropies That Results in Controlled Motion	20
2.2	Analytic model of tendon actuated mechanical metamaterials	22
2.2.1	From trusses to cellular structures	22
2.2.2	Centroid - based deformed models.	23
2.3	Empirical Validation	31
3	Skin Interfaces	35
3.1	Introduction	35
3.2	Tessellation. Search, Modification and Redesign.	38
3.3	Pattern Construction	39
3.3.1	Algorithm steps	41
3.3.2	Neutral Slope	46
3.3.3	Positive Slope	47
3.3.4	Negative Slope	48
3.4	Kirigami - Voxel Structural Compatibility	49
3.5	Matching Adjacent Anisotropies	49
3.6	From Continuum to Discretely Assembled Origami	51
3.7	Manufacturing	52
4	Applications	55

4.1	Hydrosnake	56
4.1.1	Motivation	56
4.1.2	Design	57
4.1.3	Control	57
4.1.4	Results	59
4.2	Camber Morphing Wing	62
4.2.1	Motivation	63
4.2.2	Design	65
4.2.3	Actuation Control	70
4.2.4	Simulations	72
4.2.5	Tow Tank Setup	73
4.2.6	Results	73
5	Conclusions	79
5.1	Scalability	79
5.2	Actuation	80
5.3	Simulation	80
5.4	Design	81

Chapter 1

Introduction

“Nature does nothing uselessly. If one way be better than another, that you may be sure is nature’s way.” Aristotle’s statement still resonates after thousands of years in modern academic directions as nature is a constant source of inspiration for modern engineering research trends and solutions.

Modern engineering challenges require material properties that uniform materials have difficulty providing and complex systems integration. The two main pillars this thesis found in nature’s success are its system integration strategies and its ability to generate biological materials with custom mechanical properties.

System integration

On the one hand, nature integrates systems in a way that humans cannot replicate with classic mechanical approaches [4]. Multicellular organisms are a perfect integration of structural, sensing and actuation systems, such as a unique part composed of nerves, bones, muscles and skin. Almost any kind of smart structure developed by humans shares the same system requirements: structural, sensing and actuation devices. But our classical way of integrating them is to design them all separately and pay the price of a complex integration with high cost in time and price.

As an example, focusing on solutions for transportation, mimicking the way underwater multicellular organisms travel with wavelike body motions drastically increases the efficiency of any human-made solution[47]. Many fish resonate with their flexible

bodies and extract energy from their own vortices, converting thrust out of their own drag[3] . The first successful human attempt to replicate this effect resulted in the famous MIT Sea Grant robot RoboTuna[48], that succeeded in the premise but was composed of more than 3000 unique parts delicately assembled with very high cost, time and labor penalties.

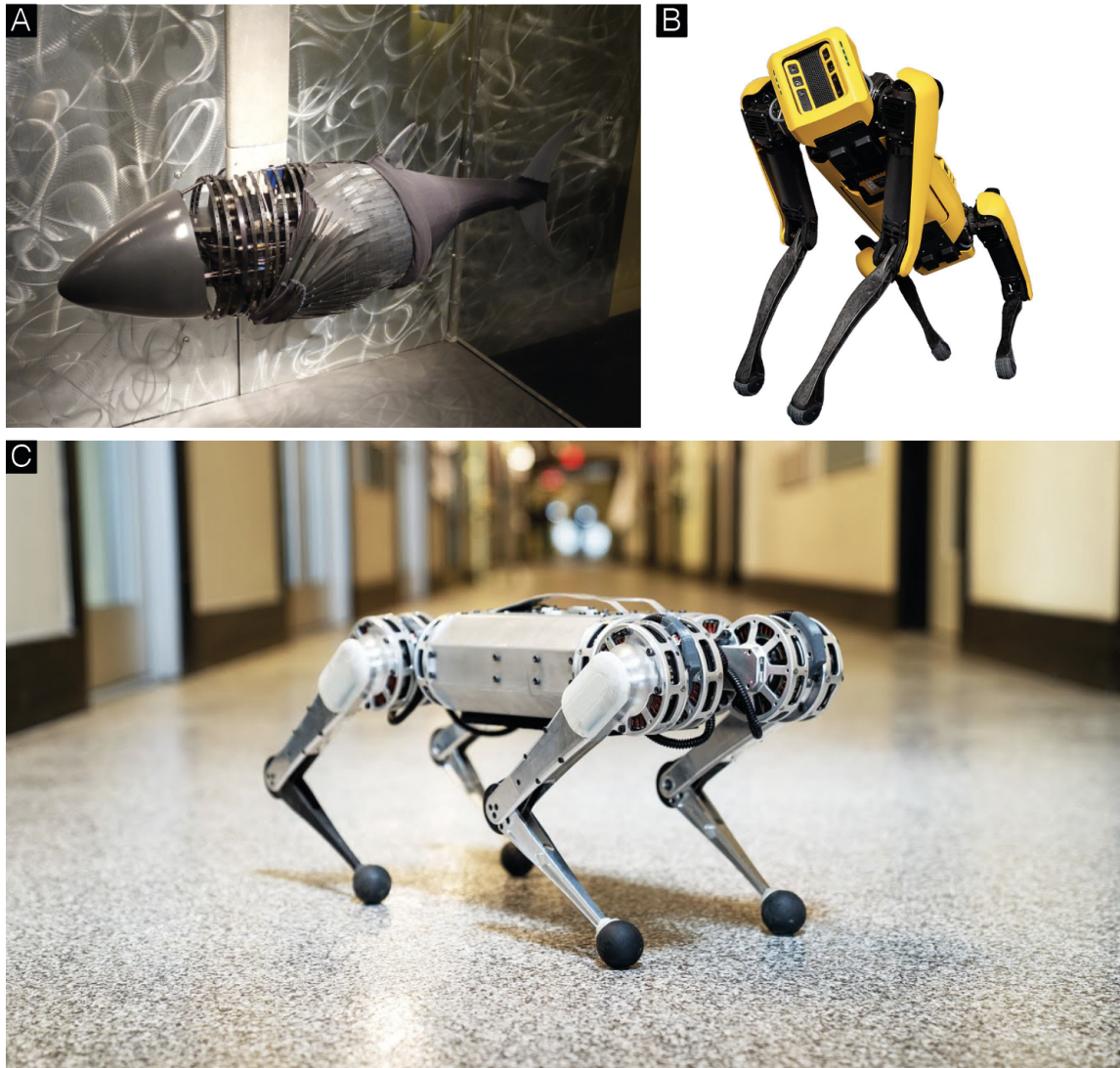


Figure 1-1: A)RoboTuna. B)Boston Dynamics Spot. C) MIT Cheetah

Another successful example is the replication of the motion of agile quadrupeds. The MIT cheetah [5] is the results of years of multiple people research. The costs of the smaller version under 10kg of payload is under 10K\$. Its industrial version, Boston Dynamic Spot, able to handle a payload of 14 kg is the results of almost 35

years of industry research and its price was 74K\$ [1].

In the 1990s, soft robotics appeared as an alternative to the classic mechanical approach. The key component was combinations of compliant and stiff materials to mimic nature-like structural movements. Examples of this novel engineering and design perspective are soft manipulators for underwater delicate sampling [13], an inflatable large-scale soft robot that moves by growing in a certain direction [20], and an entirely soft autonomous robot [49]. Soft robotics have also shown modular soft structures [33]. Continuum robotics also shares the modular mindset with an array of discrete joints with infinite DOF [7] but relying less on elastomeric materials and more on elastic deformation of their truss members[35]. Although this discipline born to provide grippers with almost unlimited accessibility for medical usage and are only conceived as beam robots, the design strategy is very interesting for this thesis because of its tendon actuation analysis.

Even though these new ways to embed structure and systems point towards a new direction that is more nature based, both fields still face issues while scaling materials, manufacturing processes or actuating their models. [28]

Materials

On the other hand, nature uses geometry to improve and customize material's mechanical properties. Intricate cellular structures appear in body zones where light weight and high stiffness are needed [40], as for example in bird's beaks and bones. Those architected materials are driven by their geometrical composition rather than material composition. One of the first sources of inspiration was how nature generates at low scales cellular solids, composing very light materials with a high stiffness value, as inner bones. This inspired researchers to make state of the art foams; it is very difficult to distinguish a microscopy of human vertebrae and polyether foams. This research field popularized complex truss structures and even allowed architected materials to behave in ways that cannot be found in nature. Metamaterials have shown negative Poisson's ratios [2], chirality[32], custom electromagnetic behavior [25], highest value of relative density-stiffness [11], and nonpositive thermal expansion [2].

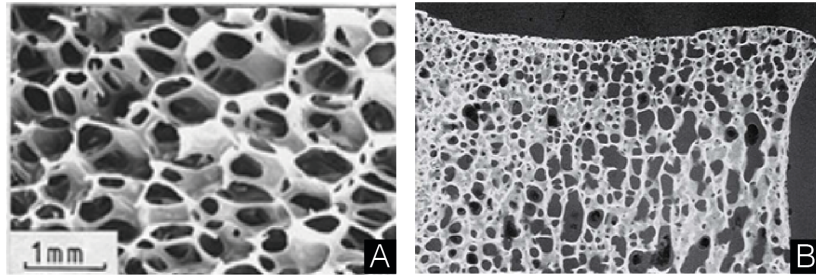


Figure 1-2: A) Polyether Foam. B) Spine bone SEM. Images taken from [14]

The appearance of Digital Manufacturing enabled the masses to manufacture those complex geometries[16]. Architected materials greatly benefited from this new building strategy. It allowed to start thinking about the possibility of encoding information into the material. Lattices with heterogeneous custom properties to control deformations were developed [27] or lattices printed with multiple materials to control its Poisson's ratio as desired [10]. But from a monolithic perspective, even with digital fabrication, a structure can be as big as the mean of manufacture allows and it will contain a global stochastic error that will increase as the mean of manufacture and the structure increases in size.

CBA alumni Kenneth Cheung [11] demonstrated how Digital Cellular Solids can be discretely assembled, like Lego building blocks, with no mechanical behavior penalties, offering world-record performance on Young's modulus versus relative density. Thanks to its drastically low relative density and that discrete assembled lattices can be theoretically arbitrarily large, it was also shown that these solids can be scaled up between the linear and quadratic regime [19]. What is still a challenge is the accessibility to mass manufacture its unit cell because the cost of molds for intricate shapes can be on the order of 10k\$.

A step towards accessibility and simplicity of the unit cell was given by Benjamin Jenett. In Discretely Assembled Mechanical Materials [21] a new decomposition of the cubic octahedron lattice was offered, reducing the costs of molds and parts drastically. This new faceted approach enabled the introduction of different geometries per facets,

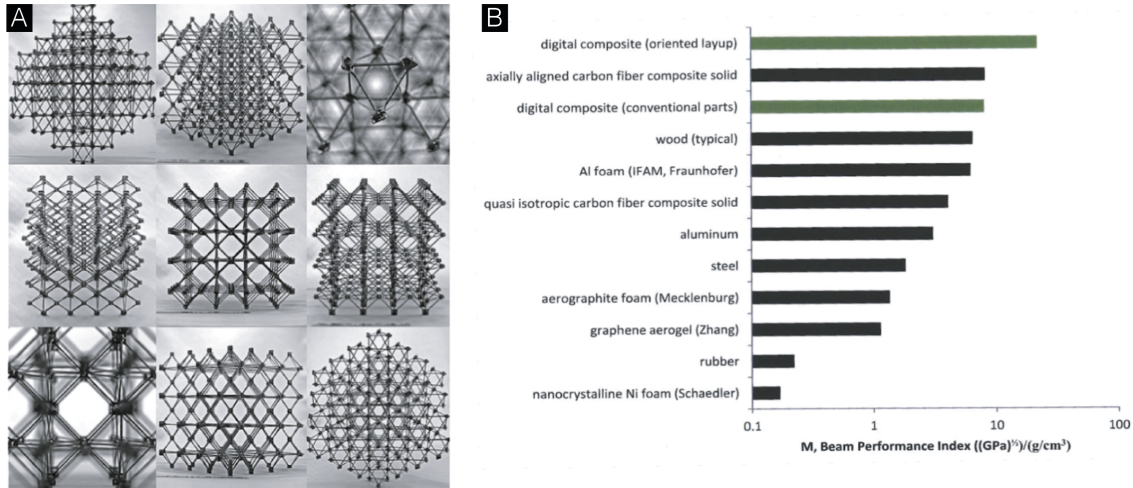


Figure 1-3: A) Kenneth C. Cheung Digital Cellular Solids. Reconfigurable Composites Materials. MIT. B) Beam performance Index for various Aerospace Materials. Kenneth C. Cheung, MIT.

to generate heterogeneous combinations of facets that make unique cubic octahedrons to assemble. This is where this thesis takes the pending work and analyzes what can be done with this construction kit.

Folding strategies are another research trend to improve materials performance. 2D processes are much faster and flexible than 3D processes. Folding showed capacity to generate metamaterials with custom stiffness [8], tailored electromagnetic properties [22], and custom thermal expansion [6]. Folding has drawn interest in fields that other cellular solids found difficult as in volume filling applications with mechanical properties. Honeycomb fillings[39], Tachi-Miura fillings [8] and free-form fillings [46] are some of the examples. Some challenges these strategies share is that they are not optimal to manufacture or assemble as, in their target planes, instead of facets, they rely on hinges.

Contributions

All the mentioned technologies serve as a base to build upon and generate arbitrarily shaped nature-like continuum-morphing structures able to scale up to regimes that soft robotics or continuum robotics find challenging.

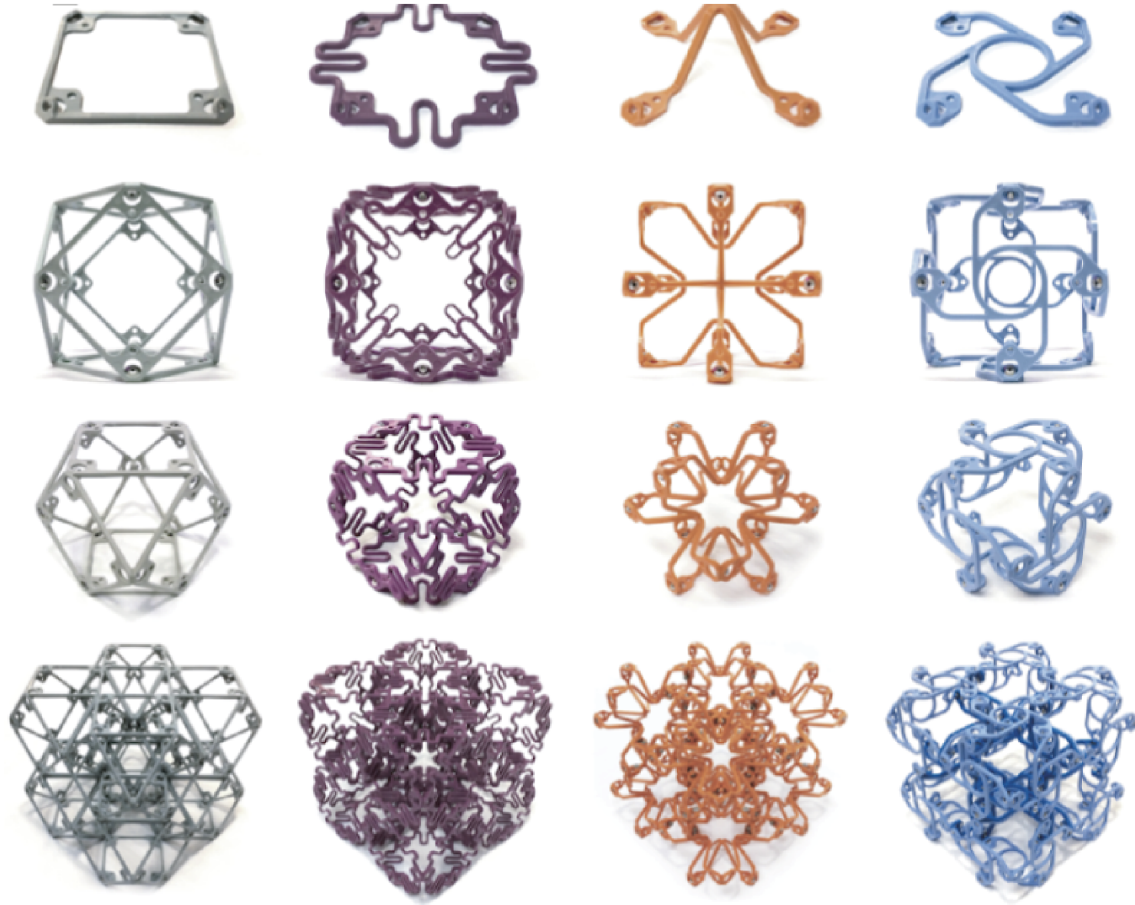


Figure 1-4: Family of voxels proposed by Benjamin Jenett et al. at [21]. From left to right, stiff, compliant, auxetic, compliant

This thesis integrates the mechanical needs of movable structures in a single process, taking advantage of the proven properties of heterogeneous digital materials and folded structures. This is a way to mimic nature's strategies by blending in the same architected material a kinematic system composed of:

- a discrete cellular solid with desirable and continuum-mechanical deformation with embedded actuation - a folded core as transition from the inner structure to the outer mold line preserving mechanical and kinematical requirements.

I will use the work developed by Benjamin Jenett et al. in Discretely Assembled Mechanical Metamaterials [21] and use those proposed geometries as the unit cell to design large continuum robotic structures with custom deformations. I will add actuation and skin interfaces to generate a compact and integrated final product.

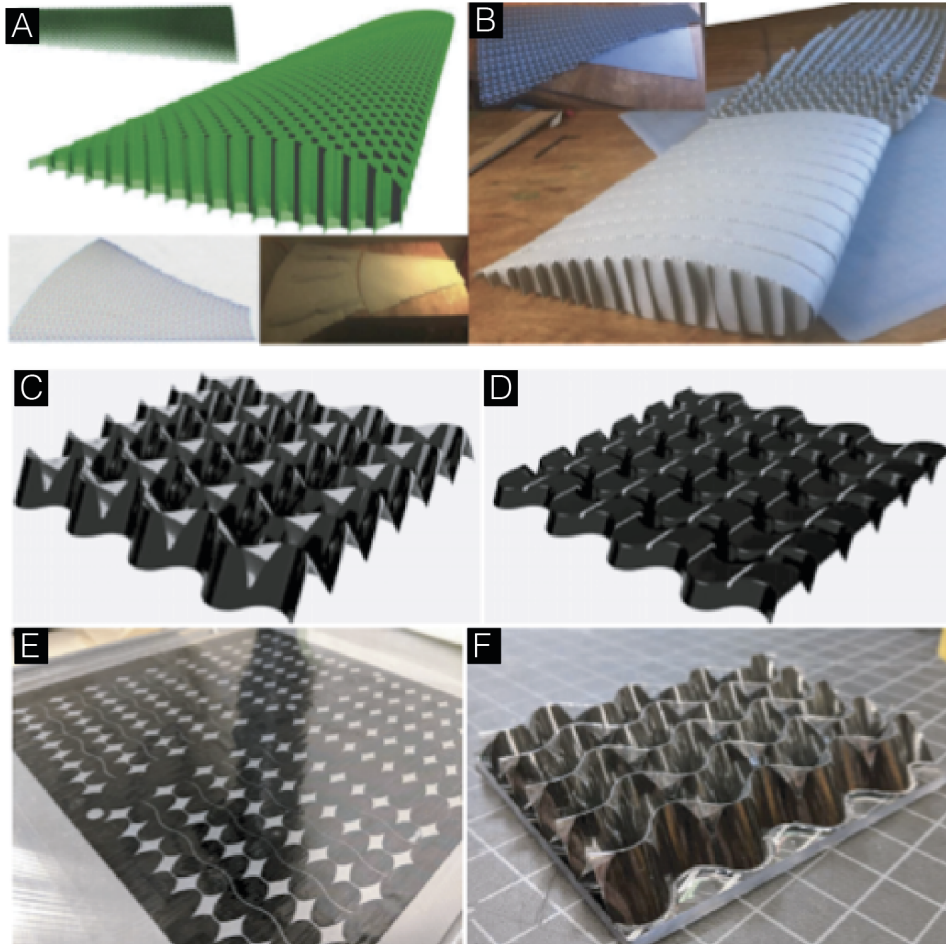


Figure 1-5: A and B) Sam Calisch Folding patterns for honeycomb with arbitrary cross section. C,D,E and F) Curved crease foldcores with impact absorption geometrical elements.

By doing that, I am proposing discrete lattice robotic structures, an expansion in dimensions with the same premise as continuum robotics but much more focused on the material system as a whole.

I start in Chapter 2 by showing actuated lattices. I explain different controlled deformations we can generate with different members of the family. Later, I focus only on two members, compliant and stiff, to analytically characterize them and predict their range of motions and load response. In Chapter 3, I explain the need for a skin interface and show the process I took to develop a novel pattern modification. I explain the mathematical relations needed to automate the generation of the folded cell and its unfolded state. I show some manufacturing techniques I use to build large,

folded cores. Finally in Chapter 4 I show examples of this approach. I show the design, manufacturing, control and testing of a water snake and a camber morphing wing, both robot length on the order of meters.

Chapter 2

Lattice and Actuation

In this chapter, I explore the possible anisotropic combinations that the construction kit can create with only two single voxel facets, a stiff and a compliant one. From a macroscopic point of view, elastomeric foams under loads can live in a linear elastic regime while their sub-structural elements (cells, beams or any sort of unit cell) don't behave necessarily linearly [14]. Knowing this feature is essential to simulate accurately the described structures. Soft bodies' actuation strategies radically differ from classical rigid-body mechanisms as they mostly rely on their linear-elastic deformation to determine their mechanical state [29]. That means that our analytical models to predict ranges of motion directly imply calculating the deformed state from the original geometry. On the other hand, classic rigid systems' ranges of movement can be geometrically calculated.

I am showing here the workflow developed to determine the shape of the deformation and the inner axial tendon tension of n by n beams based on tendon/push-rod actuation. This workflow does not introduce external loads yet. This thesis has used the commercial software Oasys GSA to calculate those cases.

This chapter will present first the different degrees of freedom (DOF) that different combinations of faces can create. Then, I show the two different alternatives I proposed to analyze the behavior of those beams under tendon-actuation strategies. Later, I show empirical parallel tests using Instron machines I developed in order to quantitatively validate those models. To sum up, I play with the simulation tool to

get a feeling of the behavior of this discretely assembled lattice when changing its mechanical properties and its geometrical characteristics.

2.1 Mechanical Anisotropies That Results in Controlled Motion

The construction kit developed for the discretely assembled mechanical metamaterials is composed of a stiff, a compliant, a chiral and an auxetic member [21]. All members of the family are shown in Figure 1-4 B. The unit cell for this discrete lattice has the shape of a cubic octahedron. This same cubic octahedron can be decomposed into 6 square-based facets. All faces share the same boundary conditions for assemblability purposes, and thus, they are interchangeable. Different combinations on a single cell can generate over the macroscopic structure axial rotations, anisotropic bending and negative Poisson's ratio deformations. Those effects can be generated locally or globally along the structure, and combinations of both will result in intricate custom movements as Fig. 2-1 shows.

For the sake of a detailed analysis, this thesis has found great interest in designing and mechanically analyzing combinations for only two facets, the stiff and the compliant.

Benjamin Jenett et al. showed a detailed validation of the mechanical properties of every family member [21]. The reason to choose only these two members is because of their different elastic modulus over the same geometry, as that of the stiff one can be 10 times larger than that of the compliant. have a huge interest to make controlled mechanical anisotropies of cells, generating desired paths for deformation to happen. As an example, with these two unique parts, we rapidly developed walking legs as Fig. 2-1 E and F show. This is exactly the point which motivated interest in generating larger continuum robotics.

This capacity of having controlled motion was shown by voxel robotic water structures such as the hydrosnake and morphing wing that will be deeply explained in

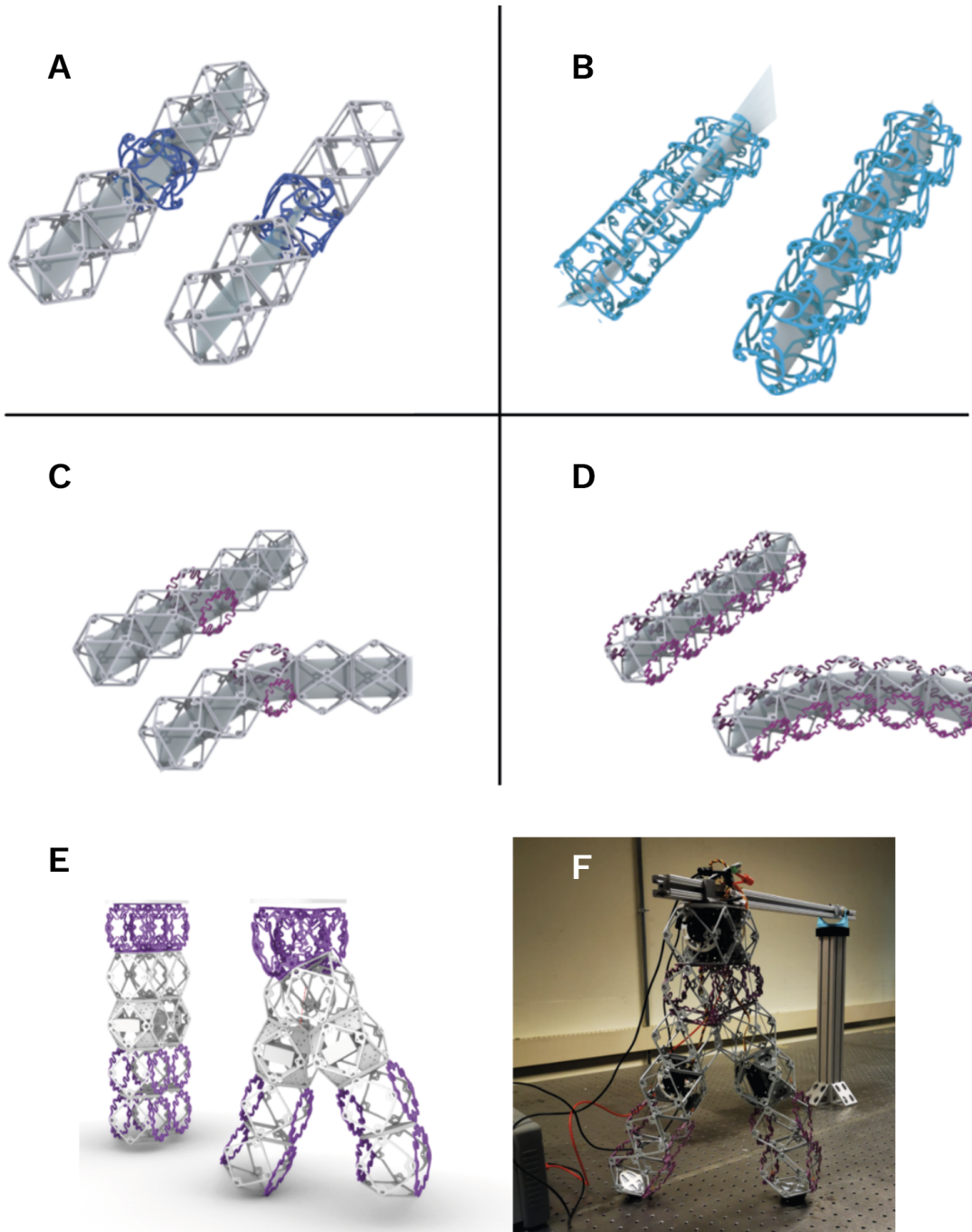


Figure 2-1: A, Local torsion. B, Distributed torsion. C, Local bend. D, Distributed bend. E, Combinations of DOF enable to generate structures with specific motion as a walker robot. F, walker robot prototype.

Chapter 4 but also by terrestrial robots such as the walker and the puppy shown in Fig. 2-2.

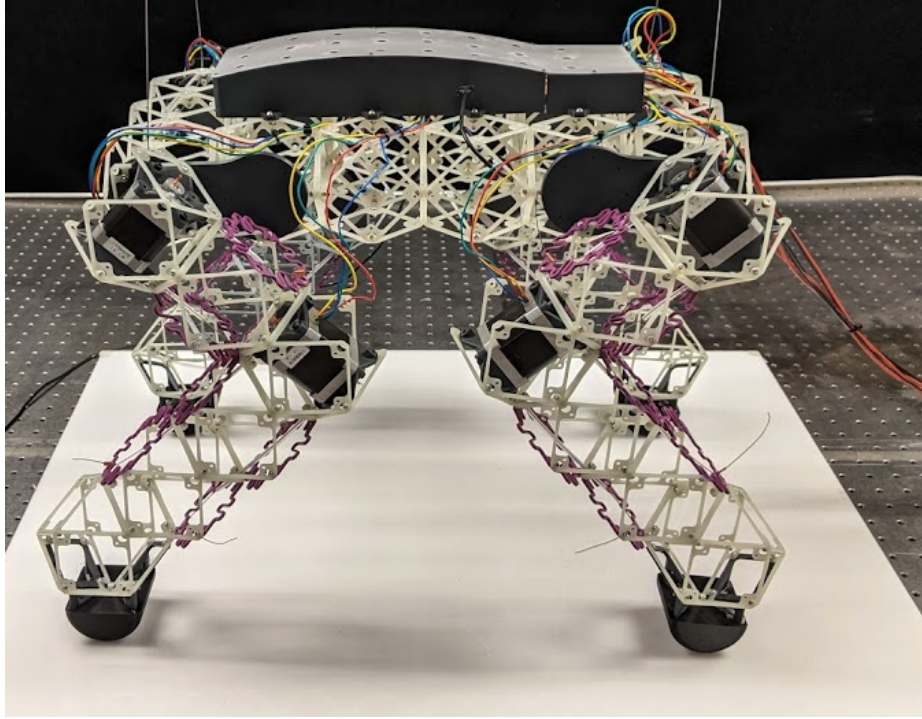


Figure 2-2: Quadruped voxel robot made by David Preiss, CBA, MIT.

2.2 Analytic model of tendon actuated mechanical metamaterials

2.2.1 From trusses to cellular structures

When working with cellular materials and trying to mechanically characterize them, literature tends to simplify the analysis by layers of abstraction. This approach shown by Gibson, Lorna J. and Ashby [14] describes the global properties of cellular materials, as for example foams, by focusing on the global macroscopic behavior, ignoring the subscale phenomena that generate these global effects. These macroscopic properties tend to have the surname *specific* and are distinguished from classic properties with an apostrophe.

Notwithstanding, in the engineering-design face of this foams, it is crucial to focus on the subscale effects to be used as fuse serial phenomena that will ensure that the global behavior of the material will always satisfy the failure over some desired zones (compressive buckling, tensile fracture or fatigue). As an example, Jenett et al. [21]

designed this construction kit with structurally invisible joints, which guarantees that the failure zone will be in the smaller area of the facets' beams.

And now, we are inducing actuation to that foam as an inner force. Tendon driven actuation analysis of compliant mechanisms is a known field from the perspective of Continuum Robotics. Since continuum robotics claims infinite DOF, discrete tendon actuation is able to use just a finite set of them [36]. In this thesis, in order to determine an analytical model, I will assume just a single tendon pulling from the base to the highest part of the beam. Thus, expanding this tool for arbitrarily located hinges once this method is based will be a simple task.

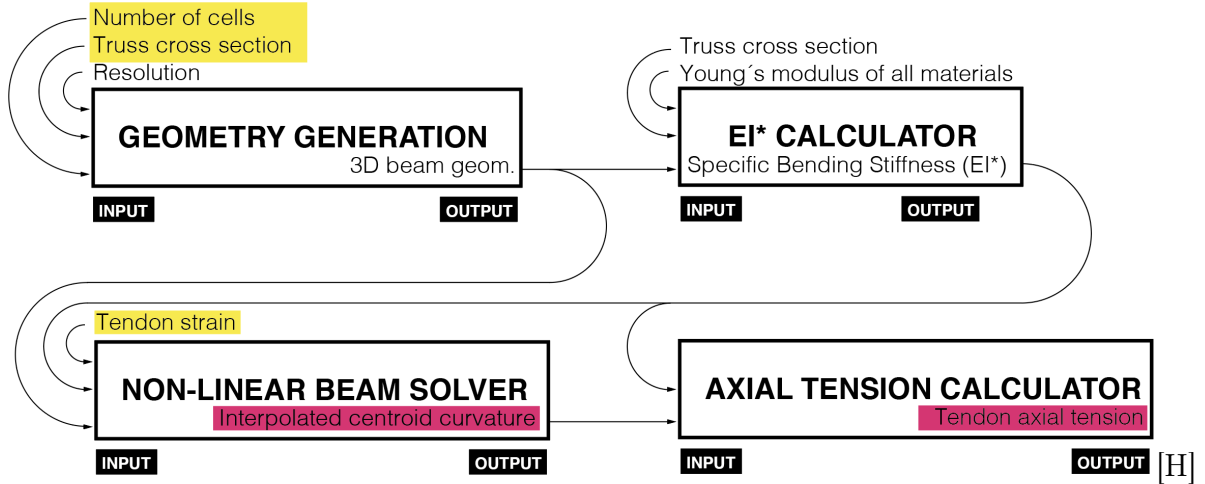


Figure 2-3: Workflow to estimate beam curvature and tendon tension given a certain strain. Yellow corresponds to general inputs and magenta to general outputs

Using Grasshopper [31], this thesis has developed a workflow (Fig.2-3) to determine curvature of the beam and tendon tension given a certain strain on it. This method enables a better shape determination of the designed mechanisms. In addition, it allows an analysis of possible actuators that would satisfy the load condition and the buckling load of any member of the truss.

2.2.2 Centroid - based deformed models.

The 3D spline that generates the center of mass of all cross sections of a beam is called the centroid. It is commonly used in continuum robotics as a reference to simplify

calculations of robots as it ideally has infinite stiffness compared to the rest of the model. This allows us to compute the centroid linear elastic model and geometrically determine the rest of the outer mold line of the robot [36] [24] [9].

In our case, the centroid of our designs doesn't necessarily have a higher elasticity modulus that would enable us to assume there is no axial deformations over it. This is why there is a need to develop a hybrid model in which the deflection of the beam and the axial elongation/compression of the beam can be computed based on its specific mechanical properties.

First attempts to determine a method were to decompose the tendon forces into a compressive load and a continuum momentum along the span of the beam, corresponding with the x axis as can be seen in Fig. 2-4.

Euler-Bernoulli method with centroid deformation.

I decided to abstract the beam as a continuum foam with a specific value of bending stiffness (EI^*) and a specific Young's modulus (E^*). For the y deflection ($y(s)$ commonly referred to as δ), I simplified the beam as a Euler-Bernoulli beam. The derivation of the specific load case we are following goes as:

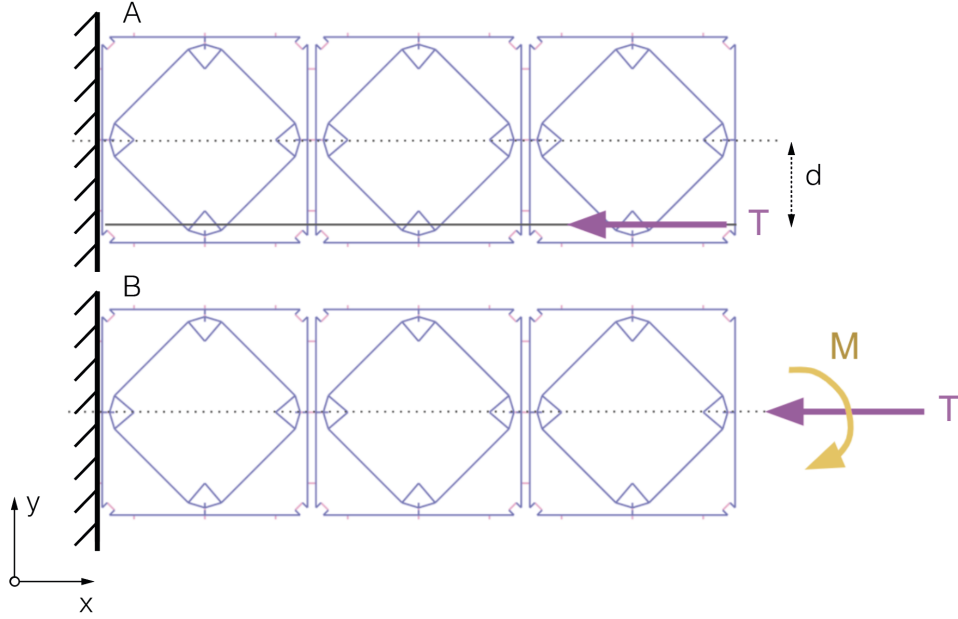


Figure 2-4: A. Tendon loadcase for a cantilever beam of 3 voxels. B. Load decomposition for analysis proposes.

$$\frac{\partial^2 y}{\partial x^2} = -\frac{M(x)}{EI^*}$$

As seen in Fig. 2-4, the tendon load T can be decomposed as a compressive load with value T applied to the centroid and a constant moment along the x direction. Calling d the distance between the applied Tendon load and the centroid, we get:

$$M(x) = T * d = M_0$$

$$\frac{\partial^2 y}{\partial x^2} = -\frac{M_0}{EI^*} \rightarrow \frac{dy}{dx} = -\frac{M_0}{EI^*}x + C1$$

$$y = -\frac{M_0}{2EI^*}x^2 + C1x + C2$$

Applying boundary conditions, $C1 = C2 = 0$

$$y = -\frac{M_0}{2EI^*}x^2, \frac{dy}{dx} = \theta = -\frac{M_0}{EI^*}x$$

In order to compute the x and y value of the centroid taking into account its compressibility, I analyze the described behavior travelling over a vector s that goes from 0 to L along it. The values of the centroid compressibility are calculated directly using Young's modulus relation.

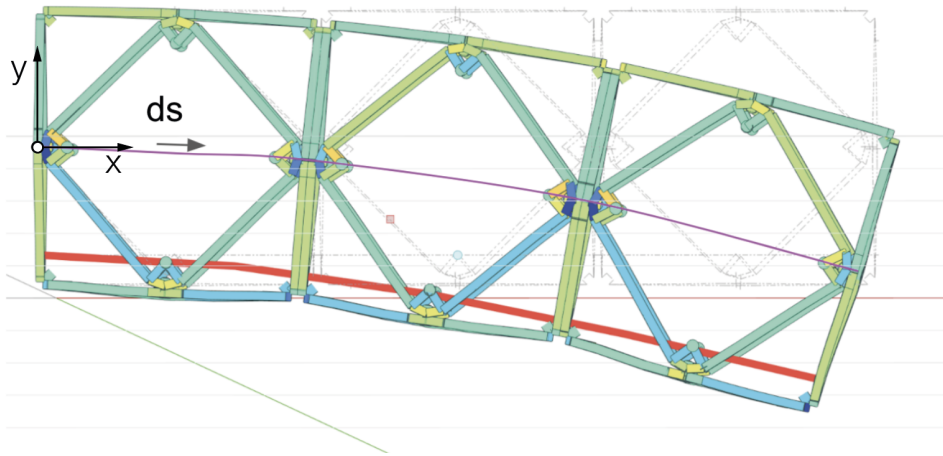


Figure 2-5: A vector S travels from x=0 to x=L to determine x(s) and y(s).

$$0 \leq s \leq L$$

$$x(s) = s - \frac{Ts}{AE^*}$$

$$y(s) = -\frac{M_0s^2}{2EI^*}$$

This method was not fully compelling for this thesis as it assumes full linearity and is force driven rather than strain driven.

Non-linear FEM solver

This thesis detected two major needs that the previous method was unable to satisfy. First was to increase the accuracy of the previous method for large deformations. This is achieved by instead of simplifying the beam as a monolithic volume, treating

it as a truss structure inside a non-linear FEM beam solver. Second, a method was needed which was strain driven rather than tension driven. Tensile-driven methods require motors able to report torque values but strain-driven controls increase the accessibility to simpler actuators capable of controlling turns.

David B. Camarillo et al. showed in *Mechanics Modeling of Tendon-Driven Continuum Manipulators* [36] a linear method to relate beam configurations and tendon displacements. Assuming in our heterogeneous beam that the neutral surface lies in the symmetric plane, we can use this method to work with the assumption that, in the absence of external loads, a tendon actuated beam forms constant curvature on its neutral surface [17][18][23][17][38], and that curvature is directly related with the moment arm and the bending stiffness of the element. I follow here the basic equations that led to this conclusion as it is relevant for this proposed method. The image shows how the 3 groups of forces that drives the free-body diagram are F_{eq} , corresponding to the integration of the contact force of the tendon along the beam, F_T as the tendon termination force and F_R as the cantilever reaction forces. Each of them generates a corresponding moment around the centroid.

$$F_{eq} = \int_0^{\phi_b} w(s) ds$$

$$w(s) = \frac{dF_w}{ds} = T\kappa_T$$

$$w(s) = R_a^e[-T\kappa_t, 0]^T$$

Being R_a^e the Euler rotation referenced to the base to any described a orientation

$$R_a^e = \begin{bmatrix} \cos\phi & -\sin\phi \\ \sin\phi & \cos\phi \end{bmatrix}$$

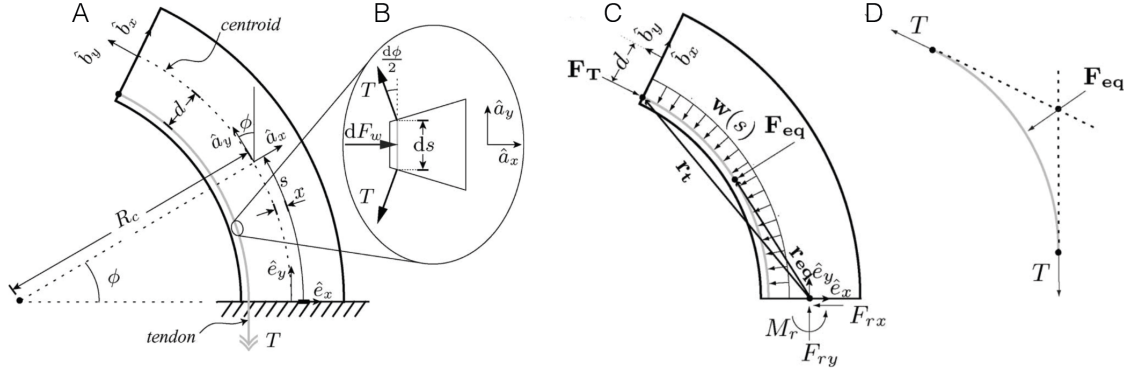


Figure 2-6: A.Cantilever tendon-actuated beam B. Differential tendon. C. FBD of the beam D.FBD of the tendon.

Source: David B. Camarillo, Christopher F. Milne, Christopher R. Carlson, Michael R.Zinn, and J. Kenneth Salisbury. *Mechanics modeling of tendon-driven continuum manipulators*. IEEE Transactions on Robotics, 24(6):1262–1273, 2008

Camarillo et al. shows how by $\sum F = 0$ and $\sum M = 0$ we can conclude that the value of curvature κ , $\kappa = \frac{1}{R_c}$ is directly dependant of the bending stiffness value and the tendon tension.

$$\text{As } \sum F = 0, 0 = F_{eq} + F_T + F_R :$$

$$F_r = [0, T]^T$$

$$M_r = -Td$$

$$M_r = EI^* \kappa$$

$$\kappa = \frac{1}{R_c} = \frac{d}{EI^*} T$$

These results allow us to enter the equation with the specific bending stiffness of the beam and the value of the curvature, and will tell the tendon load, solving the difficulties that the Euler method gave us. To feed this equation, I will compute a simplified geometry of our trusses, apply a strain to the tendon, use a non-linear solver to estimate the deformation of the beam tracking the centroid, interpolating a circle over the centroid points, and analytically calculate the tension.

In addition, I created an environment using Rhino-Grasshopper-Python that follows the described workflow. First, a script generates a simplified version of the cubic octahedron heterogeneous voxel. These geometries are sorted by the different materials that will be used. Thus, it differentiates between compliant, stiff and tendon.

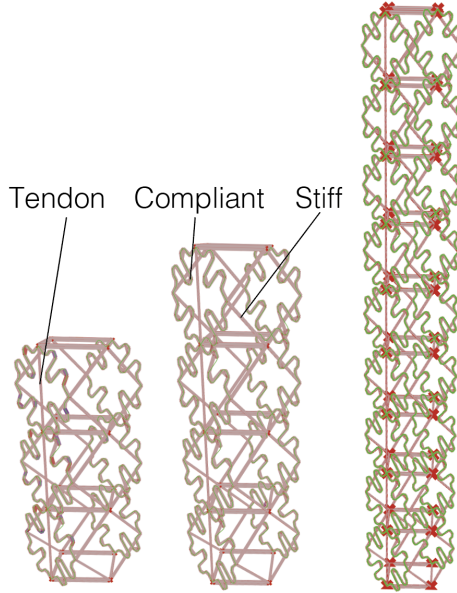


Figure 2-7: Parametric geometry generation.

Once the geometry is generated and sorted by materials and functions, I use a Karamba3D [34] nonlinear solver.

First, I developed a grasshopper tool to calculate the specific bending stiffness of the generated beam geometry. I virtually run a 3-point bending test following ASTM D4476 standard and, using beam theory for simple supported beam length l with a load P in its geometrical center, with a deflection δ , we can derive the Specific Bending Stiffness (Nm^2):

$$EI^* = \frac{PL^3}{48\delta}$$

Second, this thesis generates a model strain driven by using as load case a strain in the tendon. This strategy is geometrically compelling as we can determine the value of the tendon that will shorten easily and convert it into rotations once we know the

motor shaft to be used. All axial results of the beam elements will be valid except for the tendon. That is why I am using this method just to calculate the inner stress of individual voxel beams and its deformation. The obtained values of the axial loading from the tendon do not correspond with reality as, in a real case actuation, the strain of the tendon will be much smaller.

Once the dynamic relaxation method converges, I search with a Python script the geometric location of the centroid and interpolate a best fit circle. That will be used as R_c in the equations described above.

Using the computed value of bending stiffness, which will be a characteristic of the beam that depends on the geometry and materials, and the resultant curvature from pulling the tendon, I can compute the value of tension that the tendon will be subjected to.

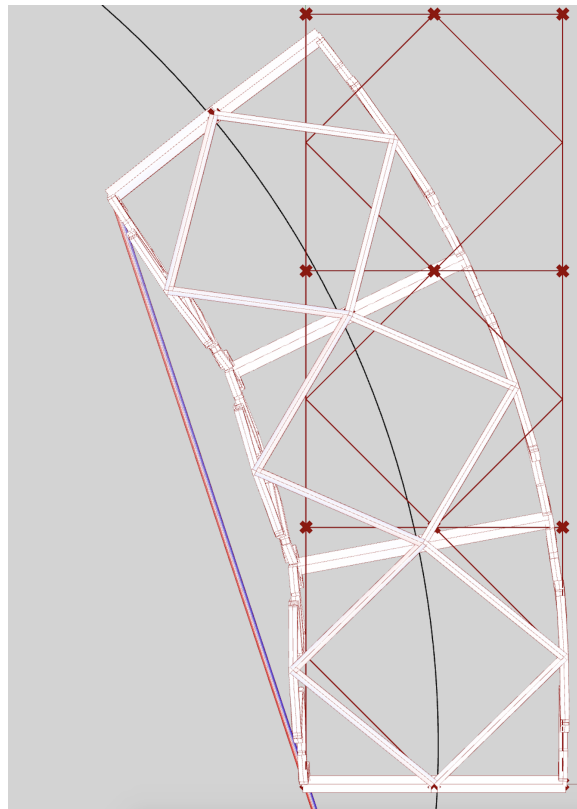


Figure 2-8: Pulling test inside Rhino-Grasshopper-Python environment.

2.3 Empirical Validation

In order to validate the model, I have built custom tooling that replicates the virtual tests developed and mounted them over an Instron 4411 and an Instron 5985. The goal was to read axial tensile loads while tracking as accurately as possible the beam deformation and to determine the bending stiffness of a certain configuration.

Validations of tension and curvature need two different systems. First, hardware serves as a cantilever base in which also the Tendon will be routed to the Instron. In addition, this hardware tooling, made out of extruded aluminum, orientates the beam to the camera orthogonally. Second, a computer vision frame is built on a Raspberry Pi 4 using the camera module, a fixed lens and written in Python using OpenCV. The Raspberry is mounted on a wall at 1.7 meters of the target beam. The full system can be seen in Fig. 2-10

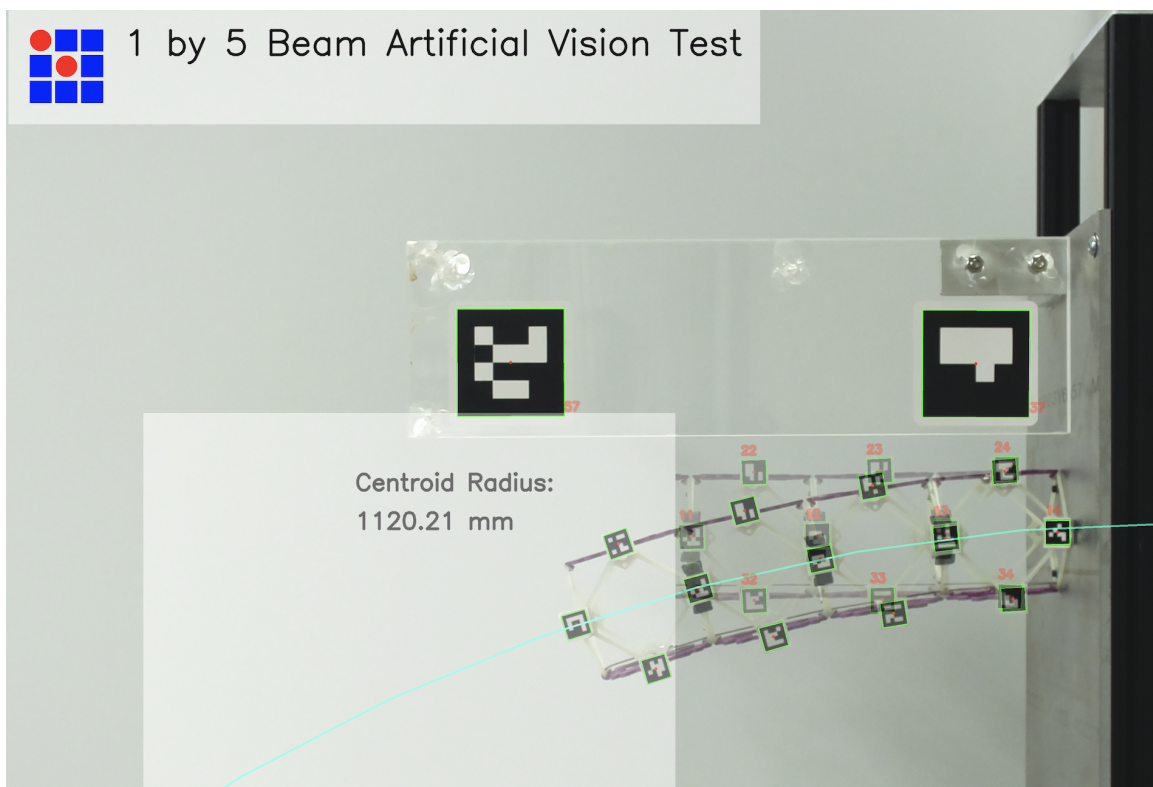


Figure 2-9: OpenCV-Python artificial vision analyzer to determine radius of centroids given a determined tendon tension.

Validating specific bending stiffness only needs one tooling system. Because of the

nature of this truss structure, I build upon the closest ASTM standard, the ASTM D4476, to determine specific loading conditions and size and shape of the tooling needed.

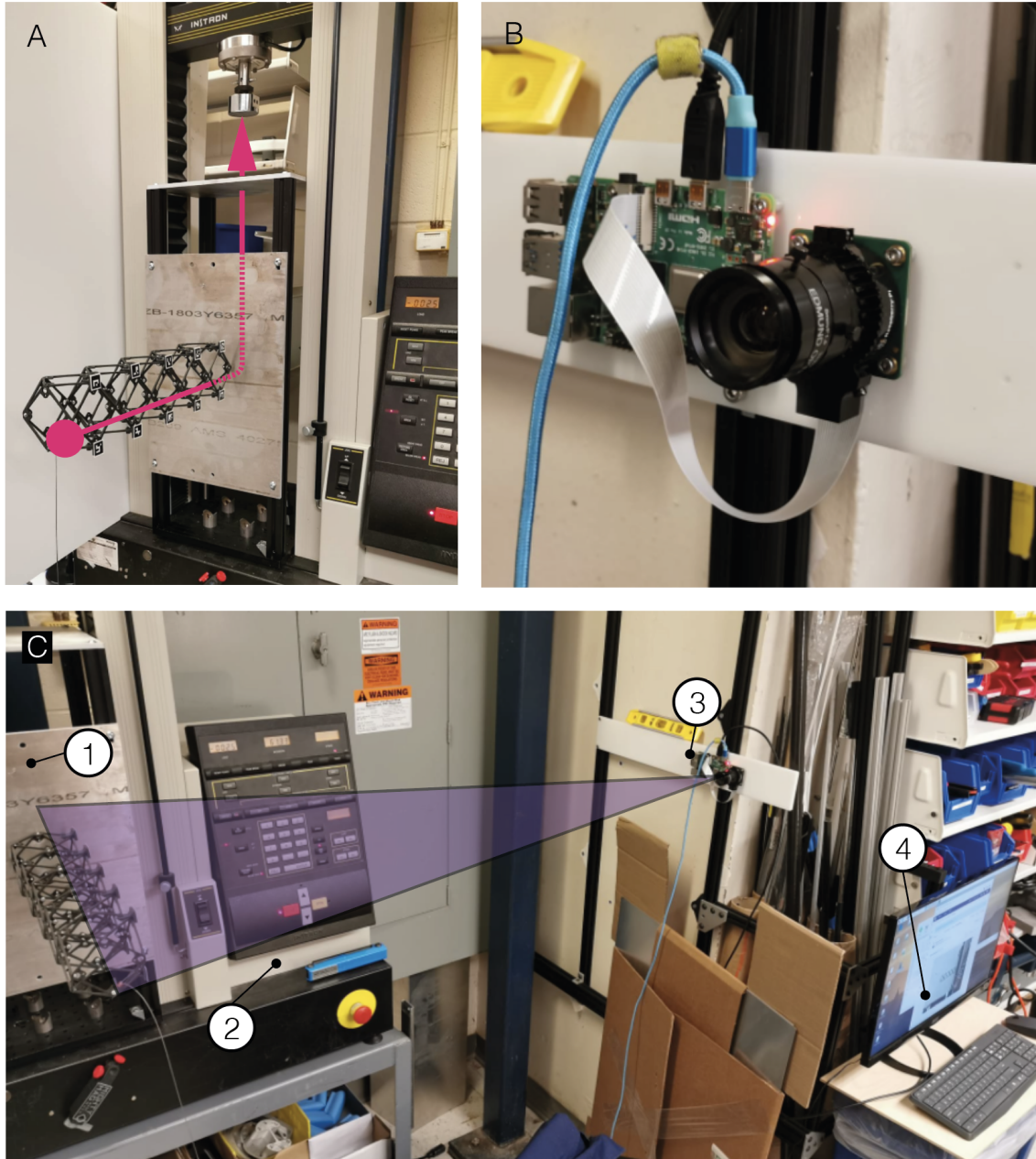


Figure 2-10: A. Tooling used to test beams to find tension - curvature correlations. The tendon (magenta) is routed orthogonal to meet the Instron requirement. B. Raspberry Pi 4 mounted in the wall with the camera module used to track motion. C. Instrument layout. 1- Cantilever tooling, 2- Instron 4411 with tooling mounted, 3- Vision System, 4- Control station.

Later, this thesis developed a computer vision system to track Aruco targets located in beams using OpenCV. This method helps to validate shape deformations of the centroid by detecting specific targets, correcting the angular deformation and interpolating a circle that fits the best the central targets. I run tests in the Instron in which the strain velocity goes to zero every 5mm. At that instant the raspberry takes a picture to later match exactly tendon tension with images taken.

With the developed tooling and the virtual tool, I proceed to perform the same experiment and verify results. As it can be seen in Fig. 2-11 we have an accurate matching of strain-tension at lower values of strain. Inside the Instron test we could appreciate how the first cantilevered voxel do sink much more than their adjacent and that impacts on the deformed visualization. On the other hand, simulations perform constant radius experiments. The deviation in radii is much higher than the deviation in Axial stress of the tendon. It must be considered that I did not took into account the rotations of the nodes in the voxels.

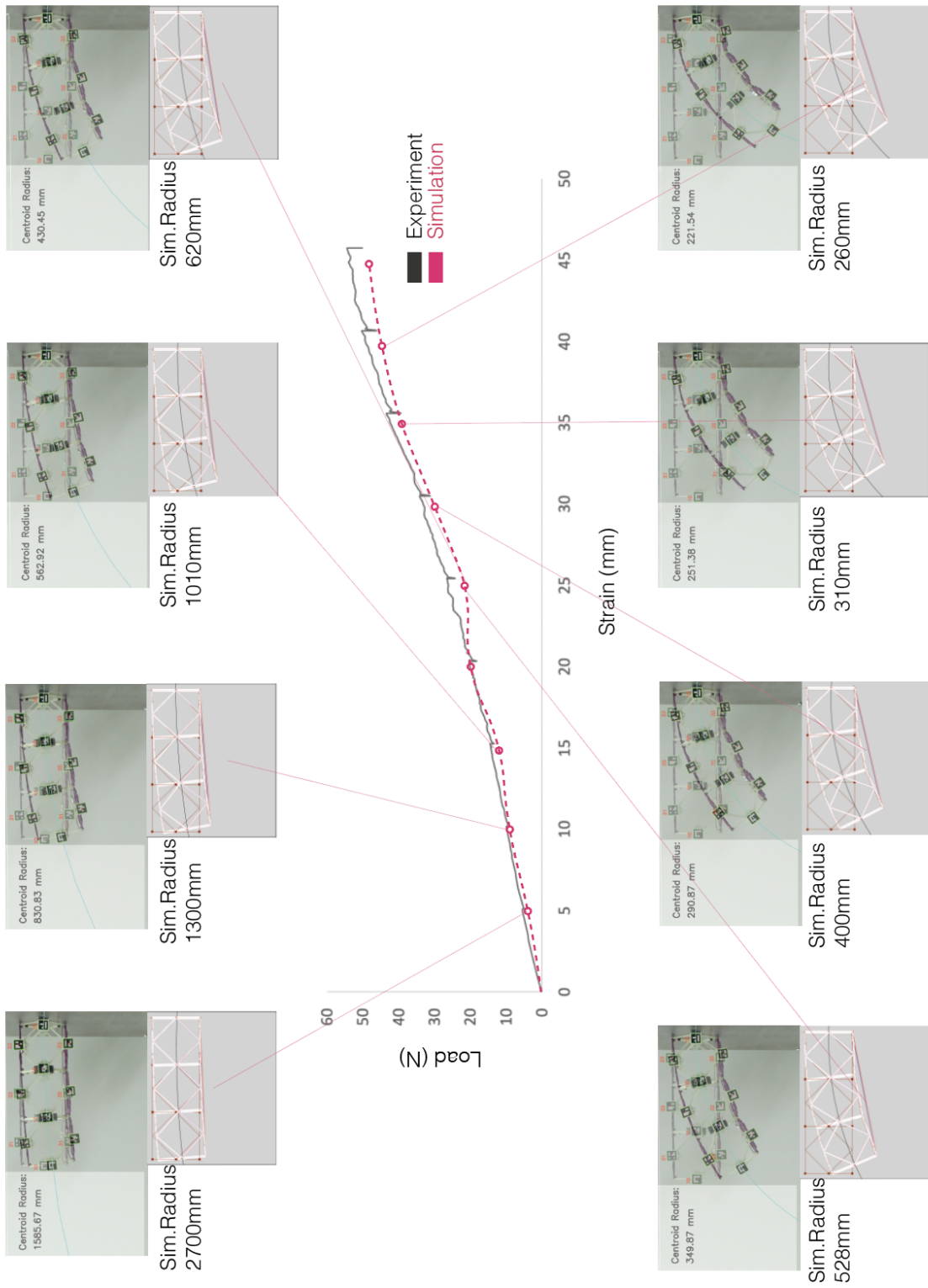


Figure 2-11: Simulation vs. Instron testing

Chapter 3

Skin Interfaces

In this chapter, I study solutions that would enable filling the gap between the structure and a continuum curvature outer mould line. Most of the solutions studied thus far that are applicable to industrial applications have a high dependency on shape. Voxel-based structures don't fill the gaps unless paying the high price of hierarchy or decreasing the unit cell. To keep the simplicity of working with one size of voxel, I developed a Kirigami structure that will distribute loads while providing any one curvature outer mold line.

First, I will introduce the problem. Next, I describe the Kirigami modification of the Miura Ori I developed, introducing the concept of *materiality*. Then, from a more generic perspective, I show the mathematical approach to automating the volume filling given two target surfaces. Later, I specify on cuboctahedral voxels for structural filling and DOF compatibility. I finish the chapter by showing some manufacturing methods used. Ultimately, I illustrate the difference between continuum origami and what I describe here as “discrete origami.”

3.1 Introduction

Most of the studies developed using voxels have a high dependency on their shape. Just focusing on this research problem, voxels oppose the ideal solution to replicate a determined shape as accurately as a monolithic structure. A building block's res-

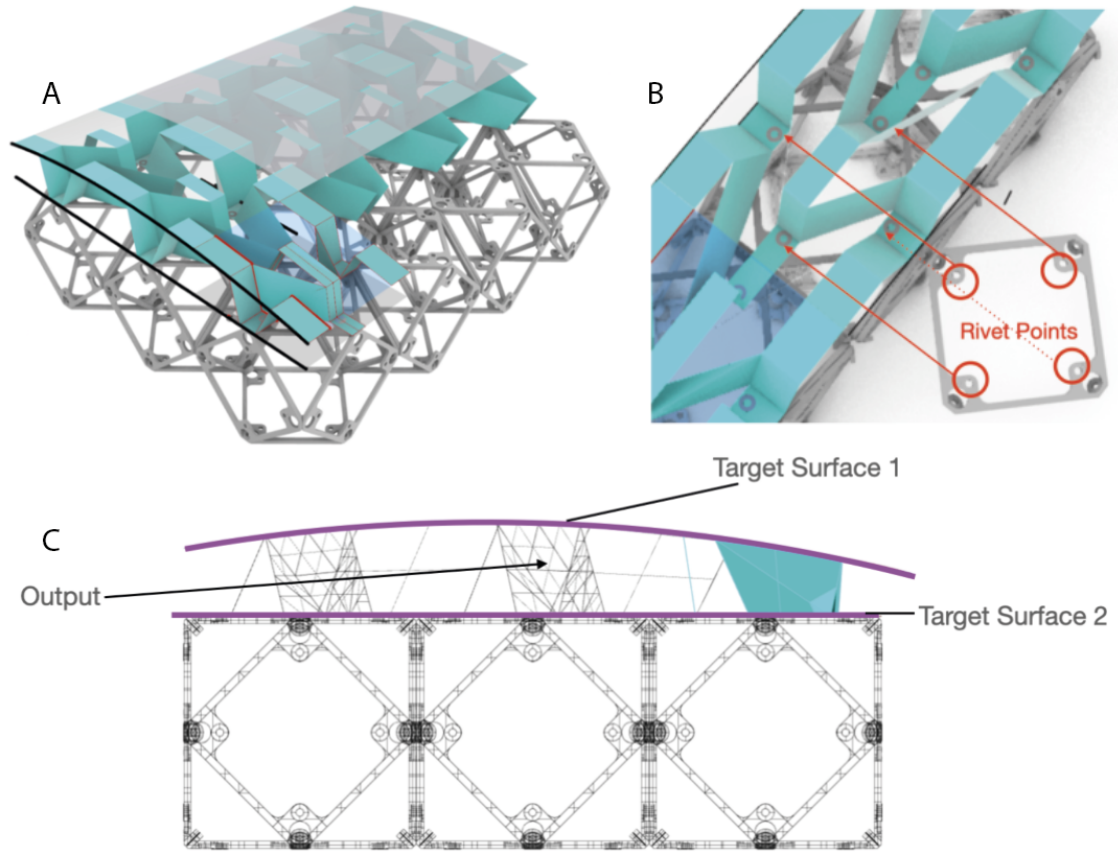


Figure 3-1: A. Kirigami core proposed by this paper. B. Footprint coordination. C. The algorithm takes as inputs Target1 and Target2 and generates the folded core and its unfolded state ready to manufacture.

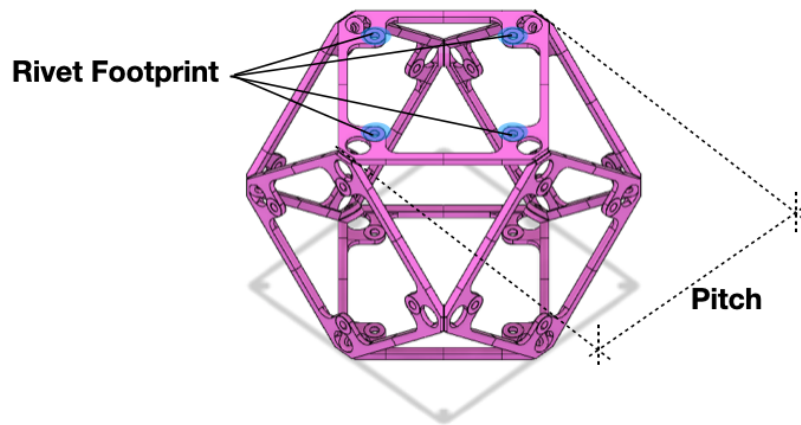


Figure 3-2: Stiff voxel. Actual voxels have 75mm pitch.

olution is in the order of its size; currently we are using a cell size of 75mm, while monolithic manufacturing solutions are in the order of microns.

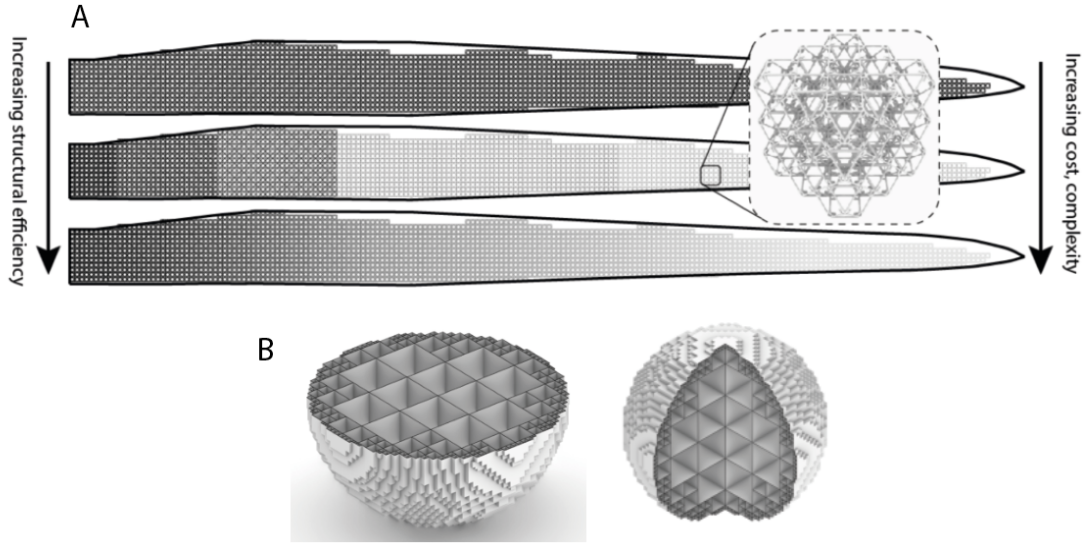


Figure 3-3: A. Volumetric fill of a discrete lattice. B. Hierarchical filling

Solving that challenge using only discrete cellular solids would introduce a solution that uses:

1. A smaller pitch value. Reducing the size of the cell will directly implies a higher resolution.
2. Hierarchical assembly. Using a finer cell as we approach the outer mold line will also yield a higher resolution.

There are reasons for not using these approaches. Both will impact the complexity of the solution, increasing the overall relative density, automation, and cost. Hierarchy, especially, would force the project to redesign faces and include more family members in order to assemble smaller cells.

State of the art volume-filling folding solutions [39] do not offer a comfortable type of folding that could be assembled into the voxel and, later, attached to the outer skin. This difficulty in assembly shows a lack of materiality. This thesis calls *materiality* to the ability of a folded structure to be assembled in the three spatial directions. Folded structures are composed of two different topologies: folds and facets. When making an array of that unit cell, it is always desirable in terms of assemblability to have a facet-facet join as they can be riveted, co-cured, glued, etc.

An edge-edge join, on the other hand, will increase the difficulty of ensuring structural bonding. Most of the rigid origami adaptative folds will die on an edge rather than a facet [8]. Ron Resch type patterns do offer facets which join on their target surfaces - but are extremely complex to fold and don't allow for mechanically attaching the lower boundary when folded, due to overlaps.

Up to this point, filling the described gap between voxel structure and skin has been done by freezing the voxel geometry, designing and manufacturing custom made monolithic solutions to adapt to slopes.

This thesis proposes a novel approach that will respect the scalability proposes and the relative movement generated by heterogeneous assemblies by utilizing a global algorithmic approach and an easy manufacturing process. The solution proposed is a Kirigami structure that, when folded, will adapt to any outer shape as its target curve but will also respect the voxel's riveting footprint in an accessible way as shown in Fig 3-2.

3.2 Tessellation. Search, Modification and Redesign.

Previous solutions shown by Calisch and Pellegrino are Kirigami [8] [39] folded cores able to adapt to any volume generated by two arbitrary surfaces if they don't intersect between themselves or the other.

But those solutions provide folded structures with one dimensional creases lying in the target surface. From a manufacturing point of view this solution is far from ideal, as it doesn't enable the physical attaching or co-curing of the core with a tangible outer skin. This thesis looks for a solution that, instead of creases, uses folded structures which generate a surface that will live in the target area when folded. A modification in a pattern must be done to transform vertex and hinges into those facets.

Firstly, I looked for patterns that already offered this materiality feature. The most interesting candidates were members of the Ron Resch family. Some of them could offer the effect I was looking for, but they weren't respecting the footprint of the voxels. Also, the folding process of a single unit cell was a challenge as it needed

a high number of folds. As folding is a parallel process, adding a hinge directly affects the simplicity of the automated solution as it adds a new independent DOF.

This is the main reason I decided to take and modify a pattern composed by few hinges and 1 DOF as the

This is the main reason I decided to take and modify a pattern composed by few hinges and one DOF as the Miura-Ori. To achieve the target geometry, a jump from Origami to Kirigami was made to gain some degrees of freedom from the rigid origami version.

To achieve that materiality we need to convert points into surfaces. The first movement is clear. As seen in Fig. 3-4, an offset was made for each of the the vertical hinges; I then extruded this point into a line (hinge) in the X axis. This tessellation is still Rigid Origami but it has lost its capacity of being flat foldable. The next step should be to extrude the new line created in the Y axis, creating a facet. This situation leads to this tessellation not being foldable anymore; here is where Kirigami became necessary. Cutting the shaded area shown in Fig 3-4 would make this 2D pattern foldable again. As can be seen, for a regular unit cell, the hinges that limit the polygon we have cut will live in the same plane, called osculating plane, with new facets we have created. This same effect happens in the Miura-Ori pattern in which alternative zig-zag creases will belong to the same osculating plane during the folding. But in our case, the new fold forces the shape of it to be different in every stage and rigid Kirigami is allowing it.

3.3 Pattern Construction

Several methods to analytically determine the unfolded solution of the Miura-Ori given a folded state have been published [15] [41] [46]. For the sake of simplicity in this thesis, I am developing the equations for this novel fold building on top of the work shown in Geometry of Miura-Folded Metamaterials developed by Mark Schenk and Simon D. Guest [41].

The space to fill is the 3 dimensional volume generated between two surfaces

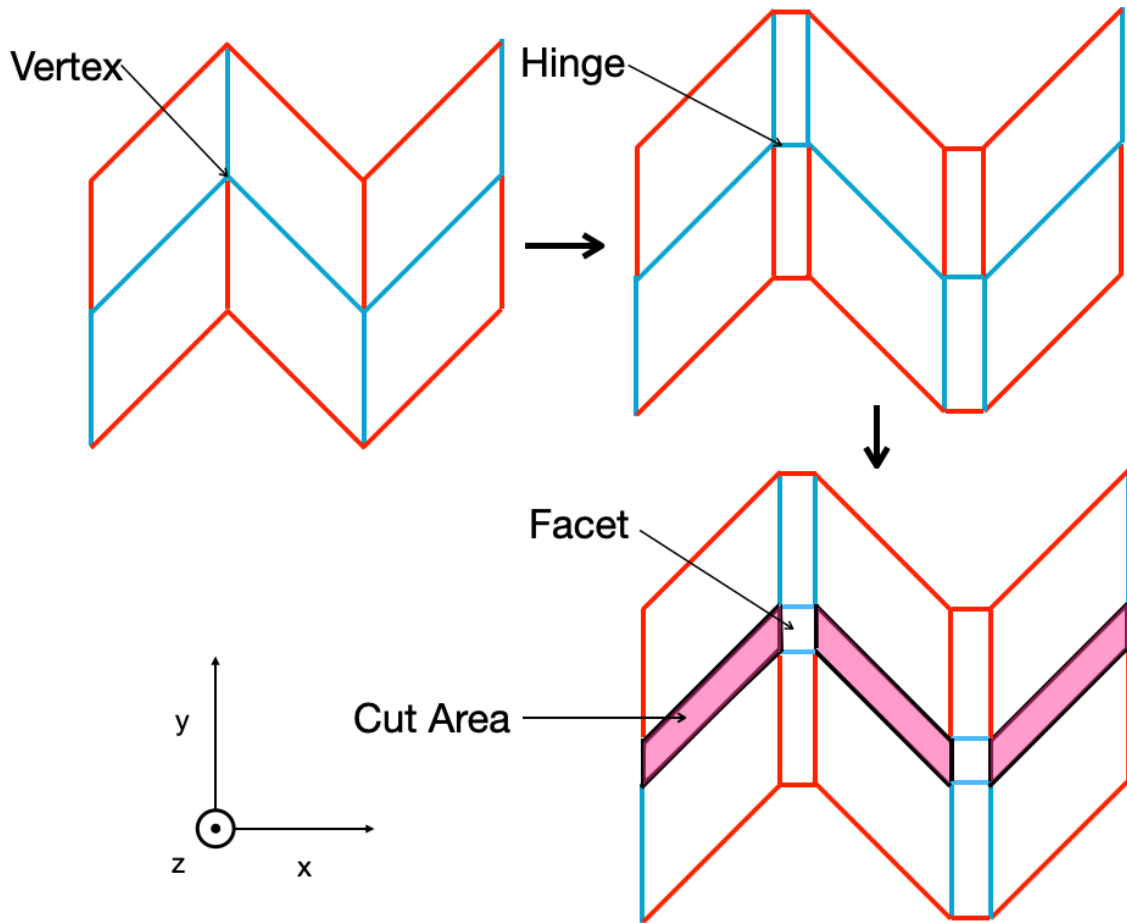


Figure 3-4: Steps followed to modify the Miura-ori into the kirigami modification

$u(x, y)$ $t(x, y)$ as shown in Fig. 3-5. This method works when both surfaces have a single curvature.

The process this thesis is describing generates a folded architected tessellation with the described novel modified Miura-Ori cell for any of the three possible scenarios: a positive slope, a negative slope or a zero value slope as Figure 3-7 shows. Next, I describe the process algorithm that this thesis generated to compute the volume filling.

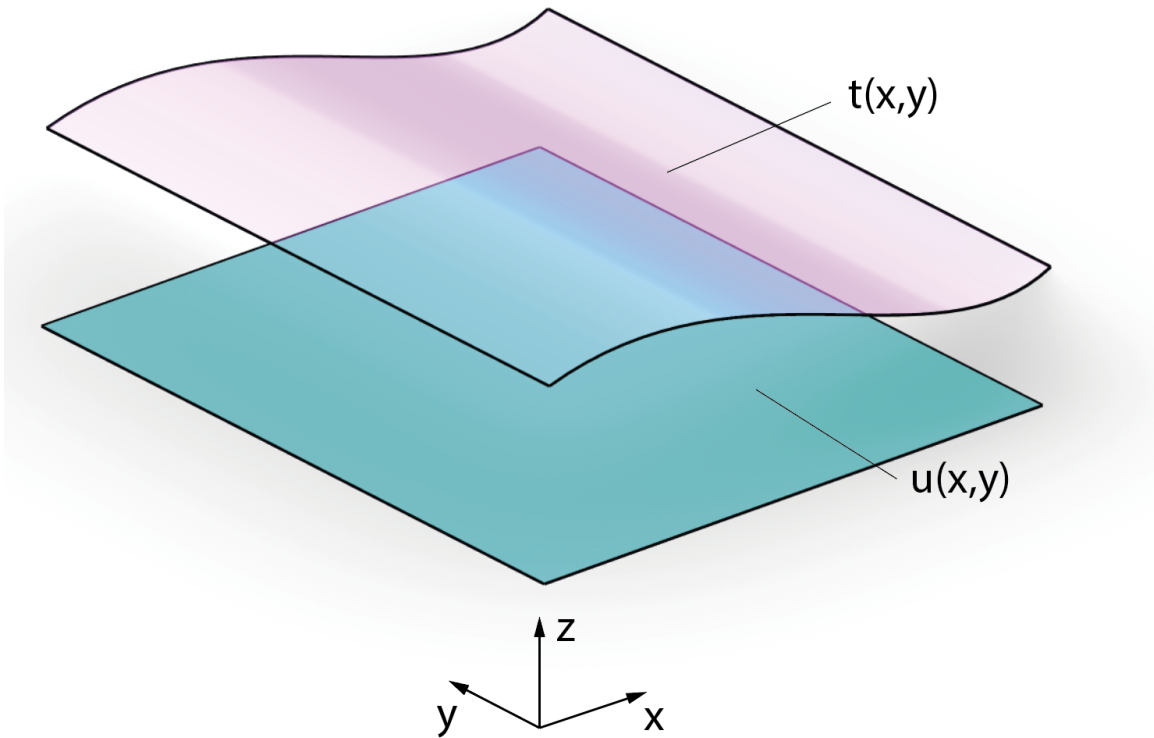


Figure 3-5: Two boundary surfaces that generates the target volume.

3.3.1 Algorithm steps

This approach fills first a folded structure as the one shown in Fig. 3-1. Previously in this chapter I showed its ability to unfold to a flat state. The method I will describe next can be applied to generate monolithic tessellations or what this thesis calls *discrete Origami* cells. For the seek of simplicity, I will start describing the method to solve a single cell and later on I will explain the steps to follow to generate either of the both shown alternatives.

This novel fold has two main characteristic parts. One is the straight corrugations and the other is the Miura corrugation. As it can be seen, the fold minimal expression can be designed as two straight corrugations with a vertical and horizontal offset in which flat surfaces are lofted on their adjacent segments. The feature that the central straight corrugation and the lateral one shares morphology is key to ensure that it is

unfoldable.

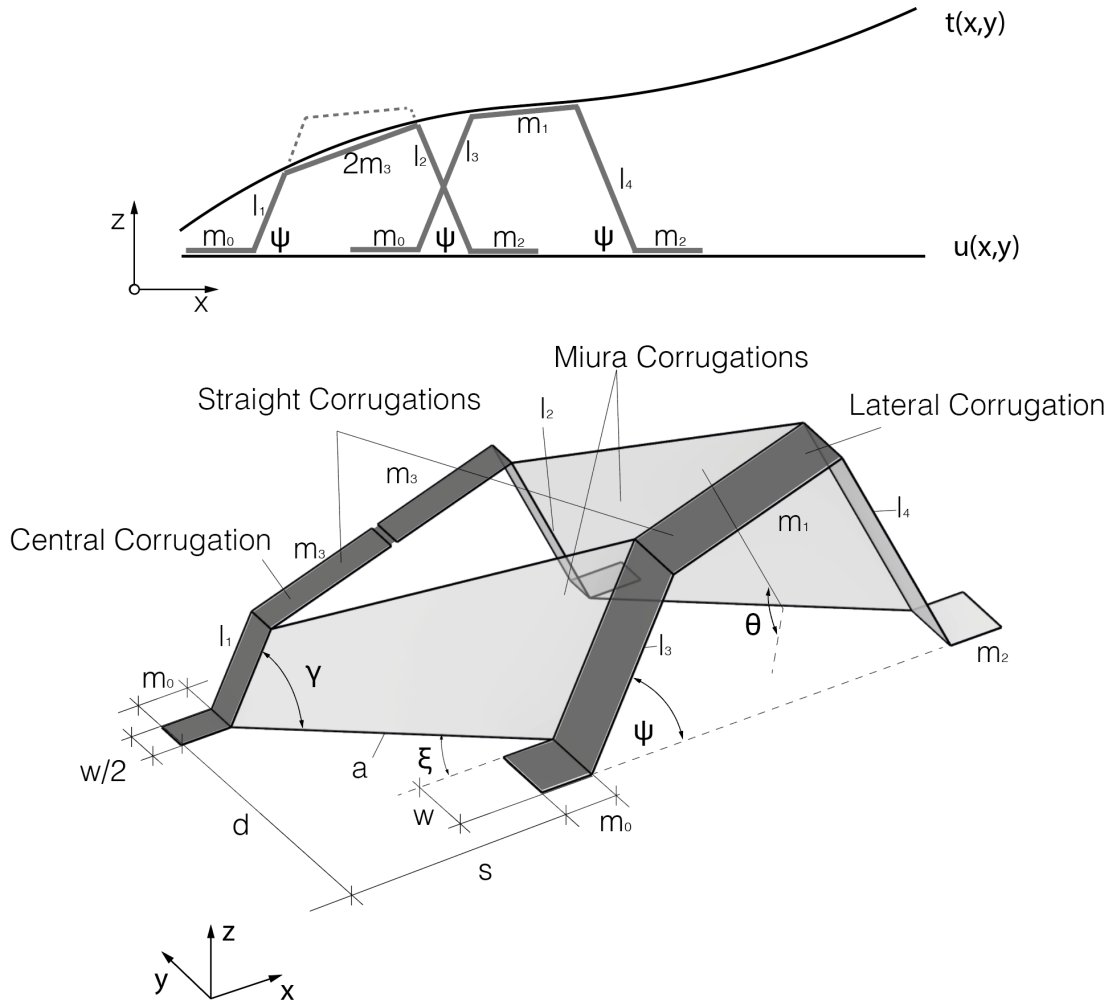


Figure 3-6: Corrugation offset method. Name variables for the unit cell.

There are some degrees of freedom we need to decide to compute the folded structure. This part of the design process makes this fold interesting to fill custom footprints and makes it flexible to adapt to custom aspect-ratio unit cells.

First, taking a lateral view as in figure 3-6, we need to trace a corrugation that when moved with an offset of s , still intersects with the upper domain $t(x, y)$. Second, once the offset s is applied, we trim the part of the straight corrugation that exceed the boundaries, resulting in obtaining the final shapes of the straight corrugations and their inherent lengths l_1, l_2, l_3, l_4, m_0 and m_2 . We now measure the lengths of the line segments of each corrugation. If the central corrugation is greater than the

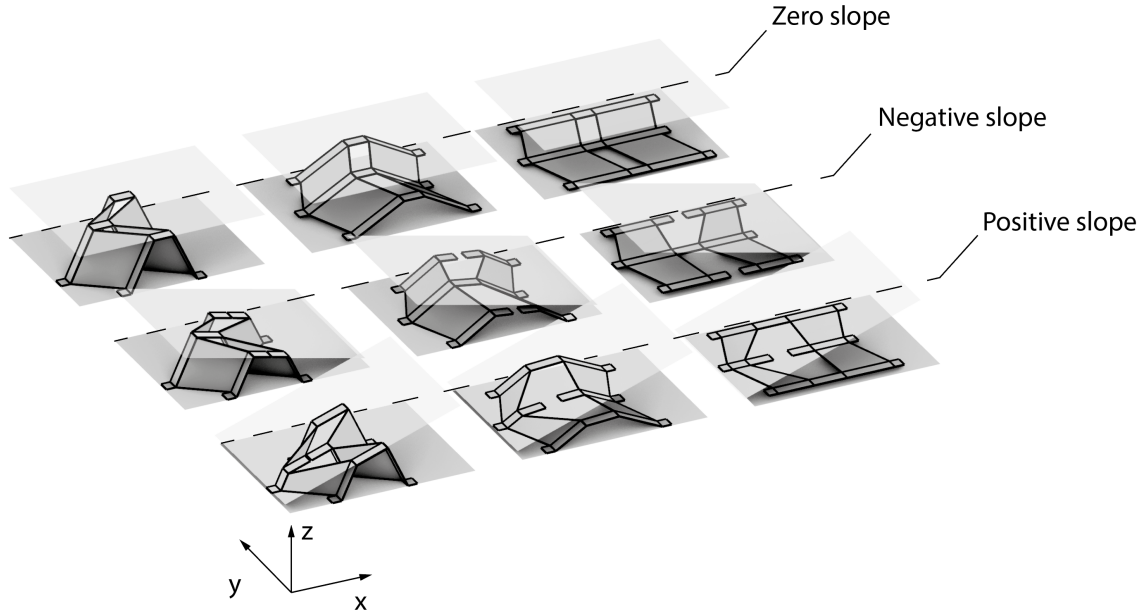


Figure 3-7: Different folded state of unit cell in the 3 unique curvature scenarios, neutral, positive and negative slope.

lateral corrugation, the cell is locally a positive slope. If it is smaller, the cell is locally under a negative slope. If the values are identical, we are in a zero slope area. For the cases of positive and negative slopes, the smaller corrugation will have a cut, dividing the top segment (the one that relies on $t(x, y)$) into two segments called m_3 . The top segment of the uncut section will be called m_1 . When working with zero-slope, the relations are simplified as there is no need to make any cut and also $l_1 = l_2 = l_3 = l_4$.

Now we move the central corrugation further in y a value of d . Also, now we decide the value w , corresponding to the extrusion in the y axis of the corrugation.

Next, we loft l_1 with l_3 and l_2 with l_4 obtaining the so-called Miura corrugations. The base segment of this facet that belongs to $u(x, y)$ is called a and will be widely used in the next steps.

Geometrically now, we can write equations to calculate ξ, ψ, θ and γ . Deriving equations from [41], we get this new relationship that sets the values for all angles as a function of ψ and ξ .

$$\xi = \frac{\pi}{2} - \text{atan} \frac{s}{d}$$

$$\theta = \operatorname{atan} \frac{\tan \psi}{\tan \xi}$$

$$\gamma = \operatorname{acos}(\cos \xi \cos \psi)$$

For the three different scenarios, I developed the equations to find all the possible vertices on their unfolded state. Being $\chi_{i,j} \in R^2$ an arbitrary vertex of the unfolded state and writing $\chi_{i,j} = (\chi_{i,jx}, \chi_{i,jy})$, I derive in table 3.3.1 equations to compute all geometric locations. The following sections of this chapter will show detailed diagrams of the three possible different scenarios, each one with its singularity.

This method can be used to fill a volume discretely filling a grid and computing and unfolding as it goes. Is it because of the nature of the sub indexes i,j for each vertex. When computing and unfolding a large number of cells, it is key to maintain the same ψ , s, d and w value in all rows of cells. That guarantees that the whole row, at its unfolded state, has the same width.

3.3.2 Neutral Slope

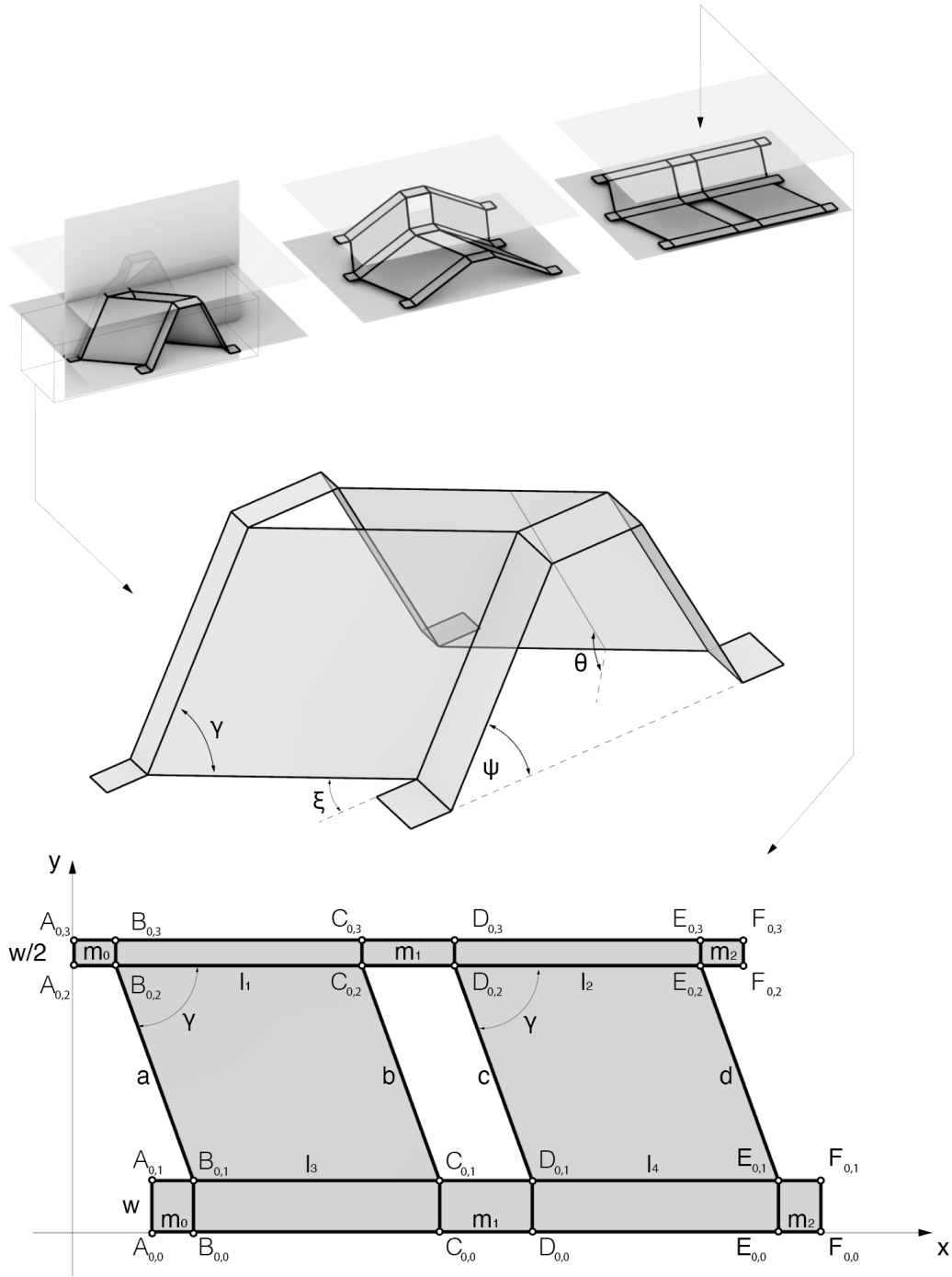


Figure 3-8: Zero Slope unit cell nomenclature. Angle definitions and vertex names.

3.3.3 Positive Slope

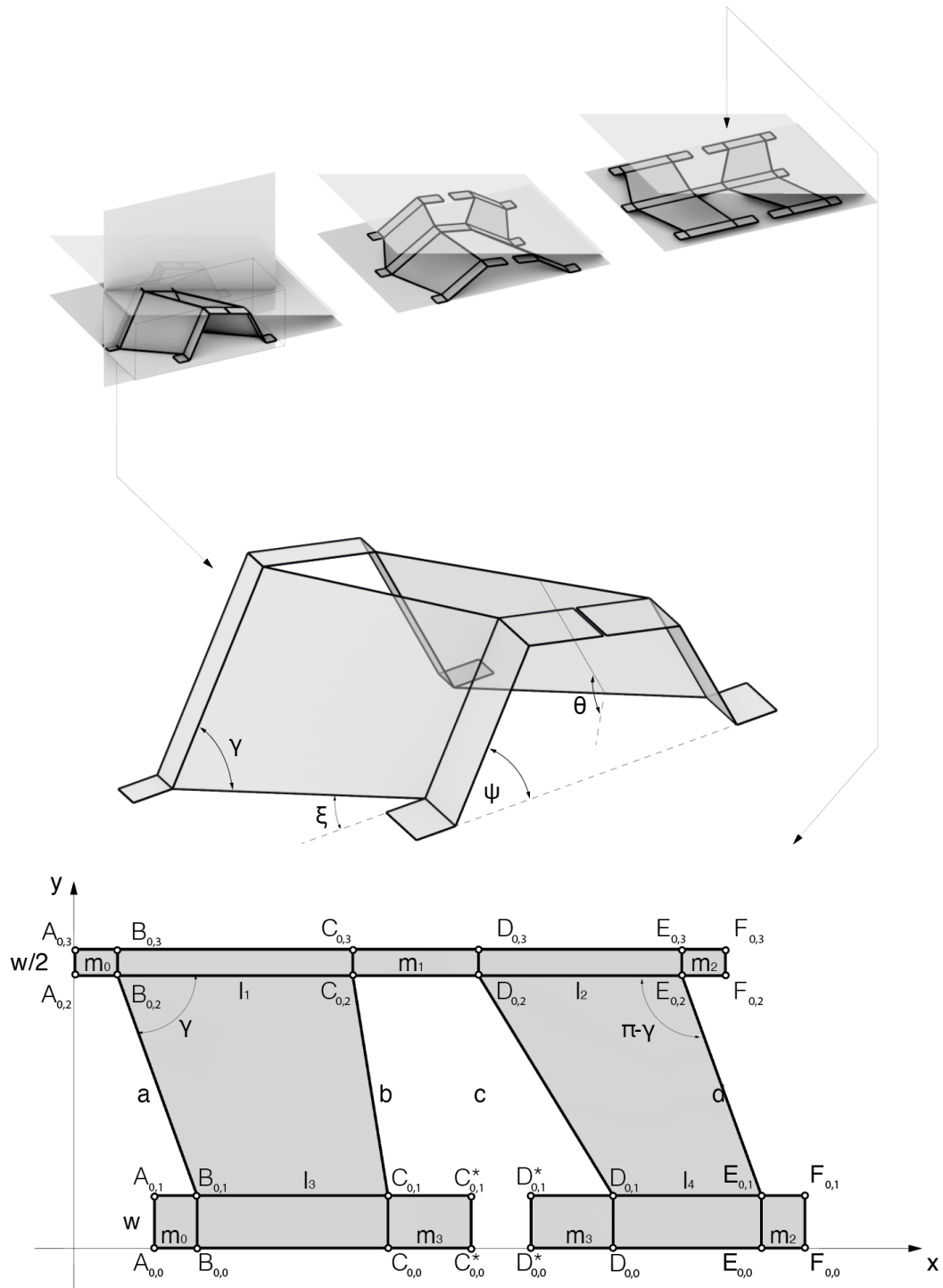


Figure 3-9: Positive Slope unit cell nomenclature. Angle definitions and vertex names.

3.3.4 Negative Slope

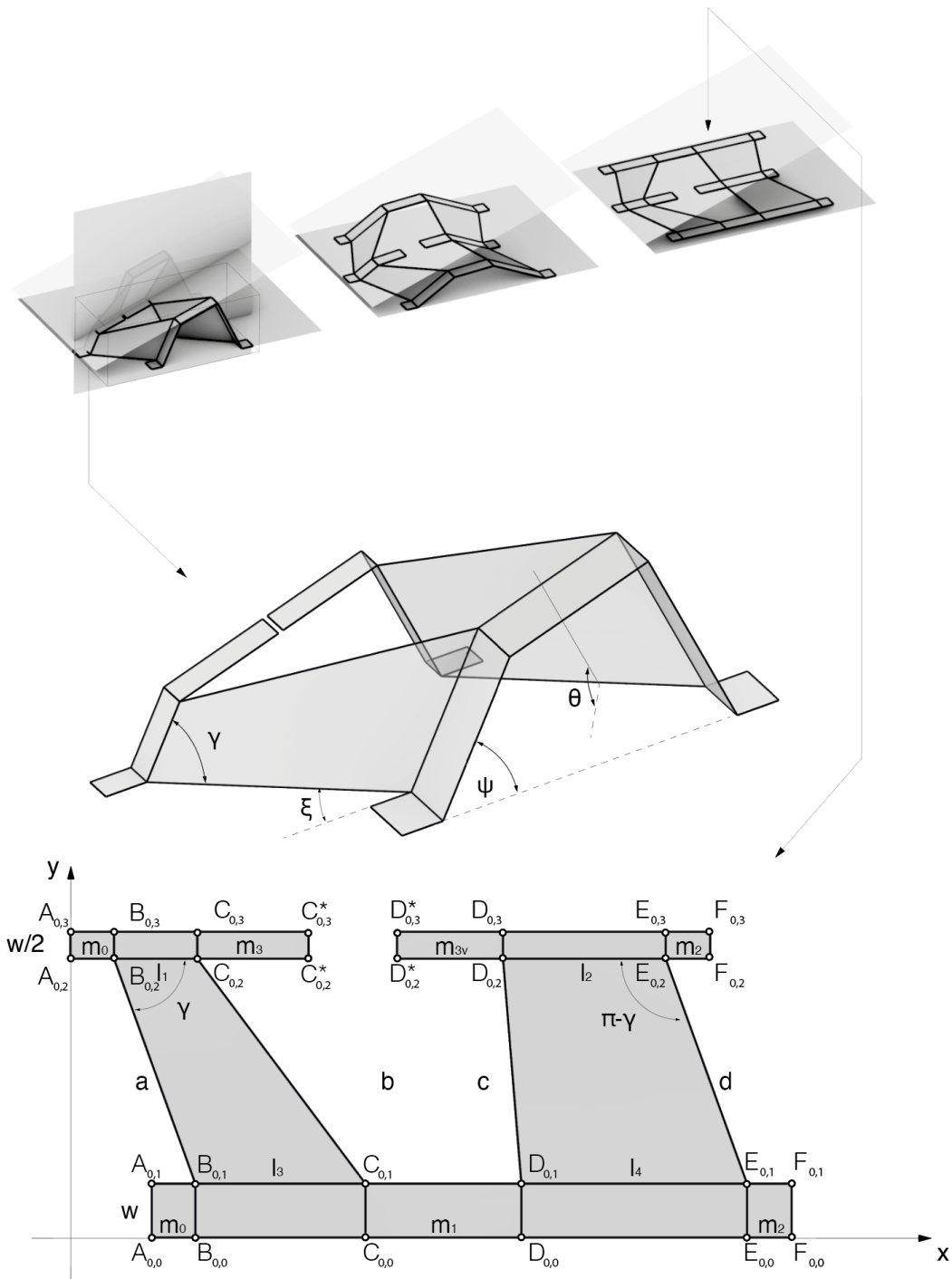


Figure 3-10: Negative Slope unit cell nomenclature. Angle definitions and vertex names.

3.4 Kirigami - Voxel Structural Compatibility

This method offer a big design space when deciding the shape of the footprint of its folded state. This feature is highly interesting for cases in which there are determined geometrical constraints to assemble the folded core with a base. As an example, in Fig. 3-2 it can be seen how voxels have on each face 4 rivets points. I can decide that my folded structure will generate facets over all them, imposing the right values for ψ , m_0 and w .

As an example, in Fig. 3-17 here I fill the gap of a torsion box with its outer mold line using the algorithm. A detailed picture of the strategy to match the footprint can be seen in Fig. 3-1

3.5 Matching Adjacent Anisotropies

If these structures could fill the gaps between the digital material structure and the target outer mold line, we need to respect the degrees of freedom of the base structure. In chapter two, this thesis explained how we can create structures with global and local hinges. If a classic modified Miura cell is placed above and assembled, we will affect the intrinsic bending stiffness of the base structure. To do so, I am proposing two strategies to provide different types of unit cells able to be completely stiff, partially bendable, and fully compliant.

The cells explained above in section 3.3 are fully isostatic structures when assembled in their target surfaces. This feature is needed when we are providing shape to digital materials meant to behave stiff. But on the other hand, that means we will prevent heterogeneous lattices to bend because of the increase in the global bending stiffness of the full assembled component. To prevent this, we can follow two approaches.

The first one, as Fig. 3-11 shown, is to add a longitudinal hinge in the Miura facet, parallel to the corrugation. This provides the pattern with an extra strain capacity along the fold. Fig. 3-12 shown deflections for the same beam with the two different

modified Miura patterns. It can be seen how the extra hinge decreases the bending stiffness of the pattern.

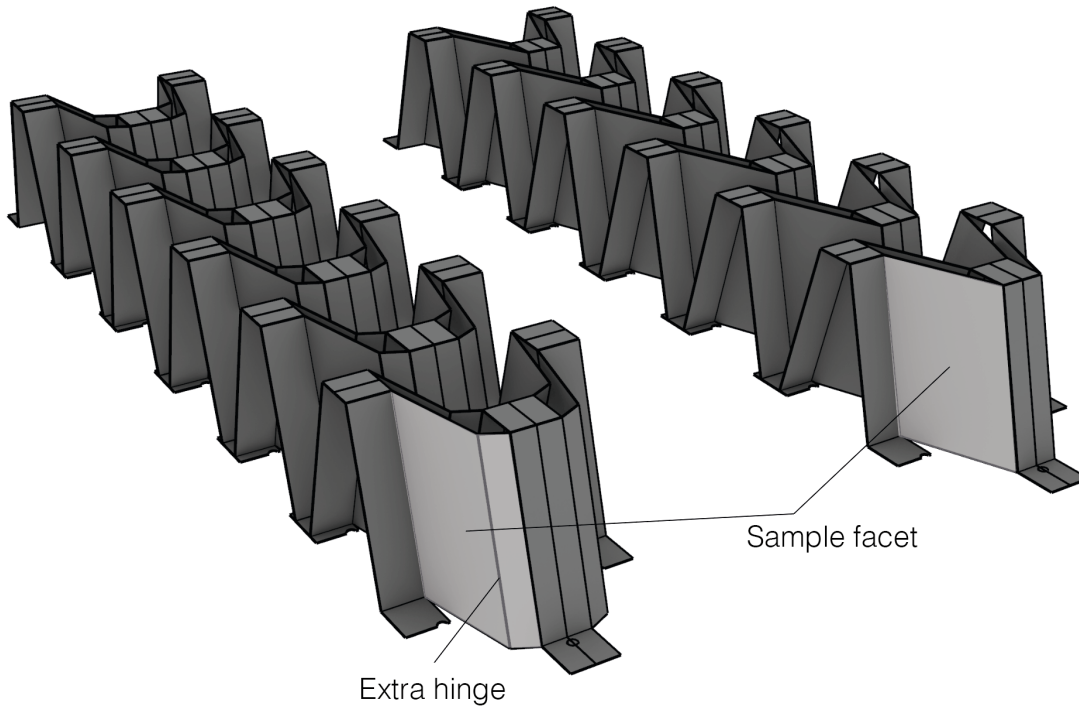


Figure 3-11: Same target, same corrugation but different Miura facet zone. There is an extra hinge that enables the fold to stretch along the pattern.

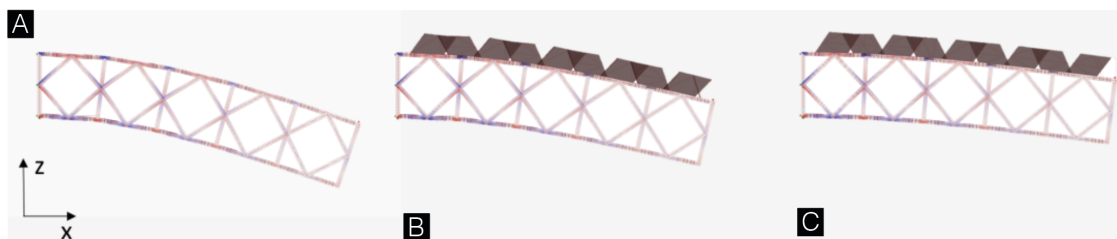


Figure 3-12: FEM with a same load in the Z axis. A) Naked beam. B) Extra-hinged modified Miura on top. C) Classic modified Miura on top.

For more extreme cases in which we want full freedom of rotation while maintaining shape, the Miura corrugations can be fully removed. In chapter 4 it can be seen that this approach was used to build the morphing wing. Fig?? shows how seems a design with stiff and bend facets.

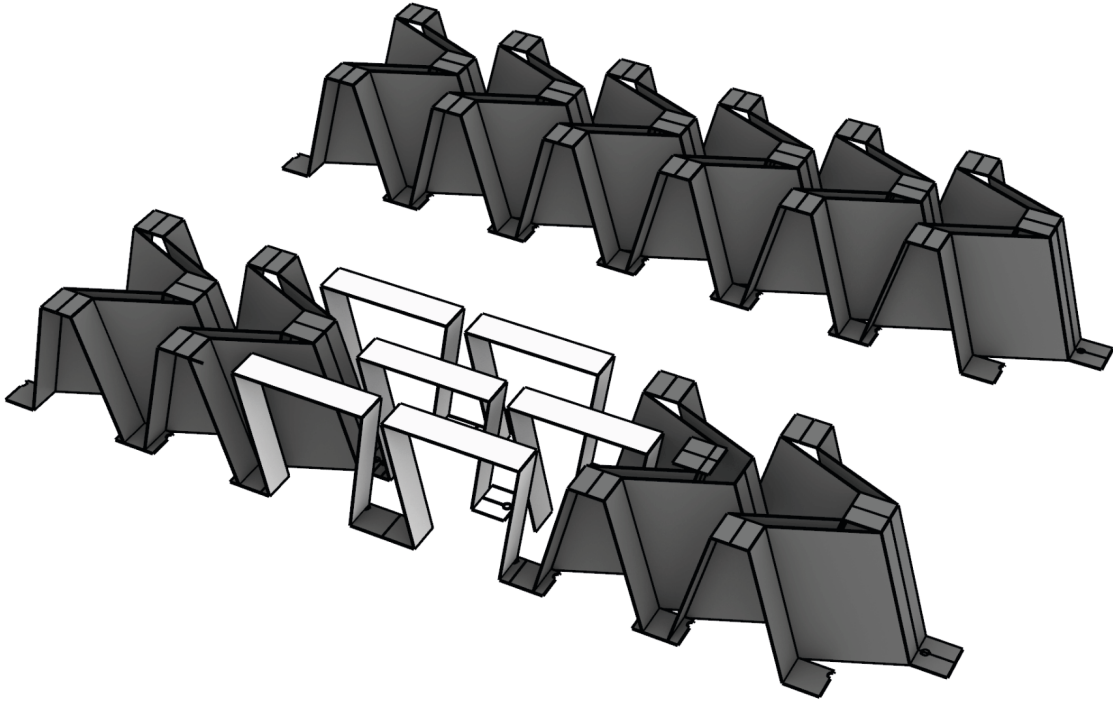


Figure 3-13: Completely stiff vs. Local bending due to half inverted exagone core.

3.6 From Continuum to Discretely Assembled Origami

As it was described previously, folding origami tends to be a parallel process. This effect has been very predominant when milling large folding cores with this new material. In order to solve that, I decided to experiment with a concept using discretely assembled origami. Taking the same premise cellular structures started to be discretized, I propose in this thesis a method to construct discretely assembled cellular origami structures as it could solve industrialization issues of large continuum folds.

Taking the simplest repetitive molecule that creates the fold, I have designed an algorithm that generates instead of continuum rows of cells, individual cells.

As an example of this method, a new version of the wing shown in Fig. 3-17 was developed using this discretized strategy as shown Fig. 3-15

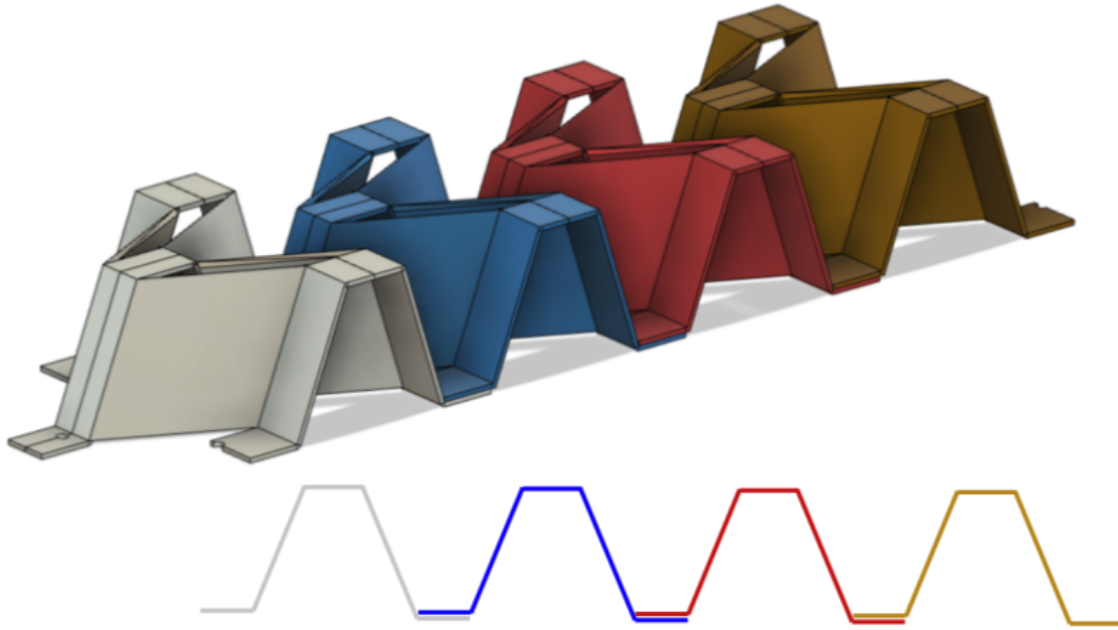


Figure 3-14: Discrete Origami

3.7 Manufacturing

First, this project chose to work with encapsulated carbon fiber in Kapton tape. This method was selected because it allows to cut prepreg sheets, encapsulate them in Kapton tape, cure it and fold it. But the complex geometries and all the needed holes made the process tedious and hard for industrialization.

Second, this project used metal folding. Aluminum sheets of 0.5mm cut in a metal laser cutter was a much faster method than the previously shown. It is needed to post-process some of the rhino workflow to generate desirable dash lines to prevent them from cracking when folding.

Folding sheets of metal by laser-cutting tiny dash lines, especially aluminum, can be a problematic process as we can easily overstrain locally in the hinge line cross-section. Laser-cut dashed lines generate such a small radius of bending that causes a local big relative strain of the material in the hinge line. The metal can enter the plastic zone regime at the hinges and that can be problematic as its properties to resist fatigue decrease. It was needed a hack for this issue.

To do so, I found an aluminum composite called Hylite by the manufacturer 3A.

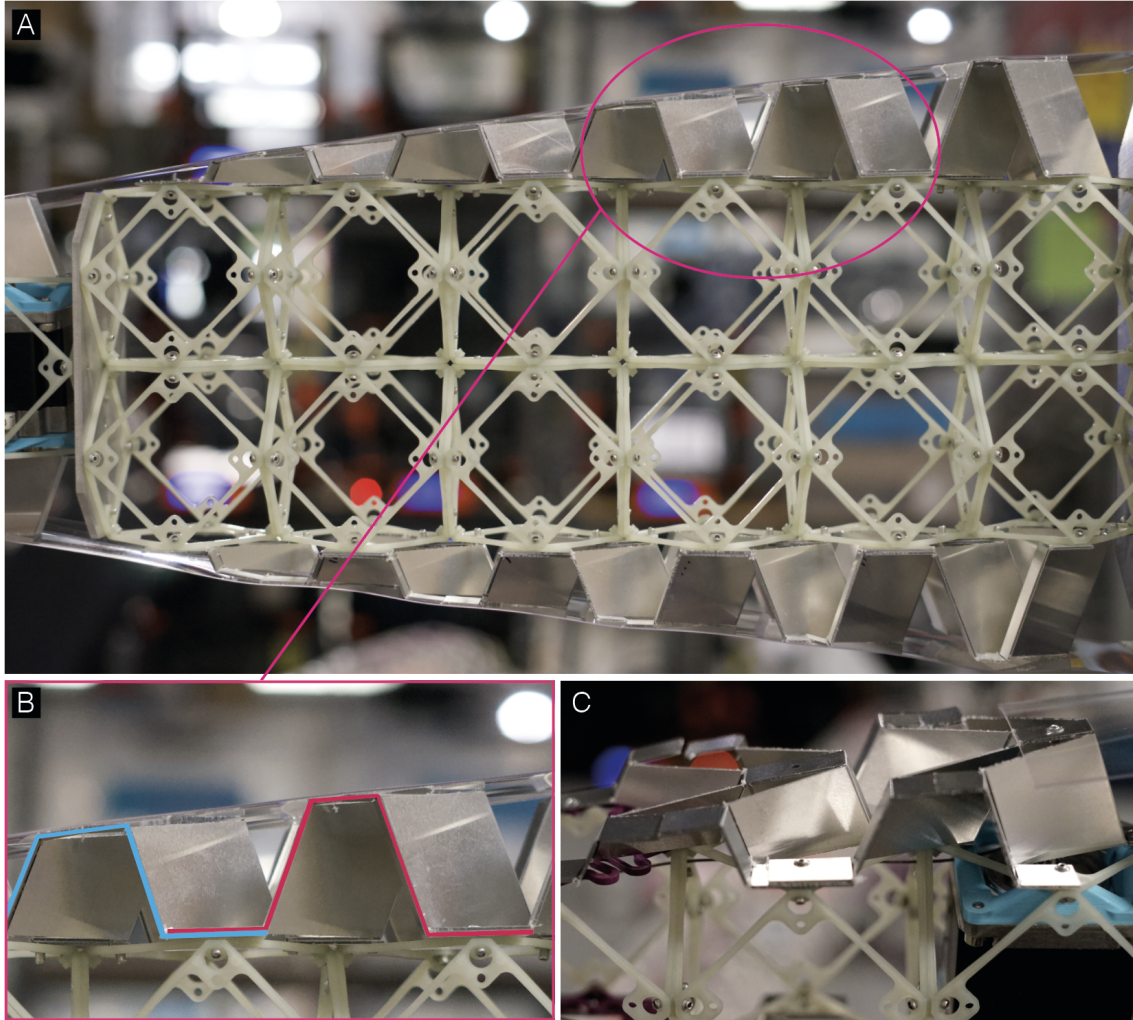


Figure 3-15: Discrete Origami

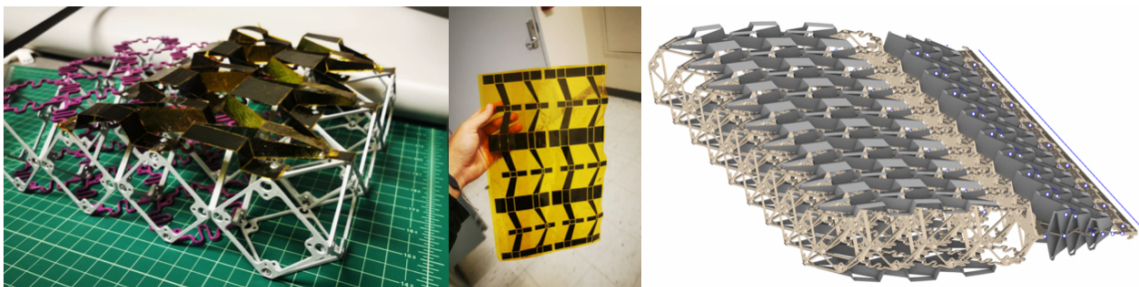


Figure 3-16: CFRP

It is a sandwich material composed of a polypropylene core of 0.8mm encapsulated by two layers of 0.2mm of aluminum. This lightweight composite material preserves the elastic module of aluminum (70GPa) but only weights one-third of the same thickness

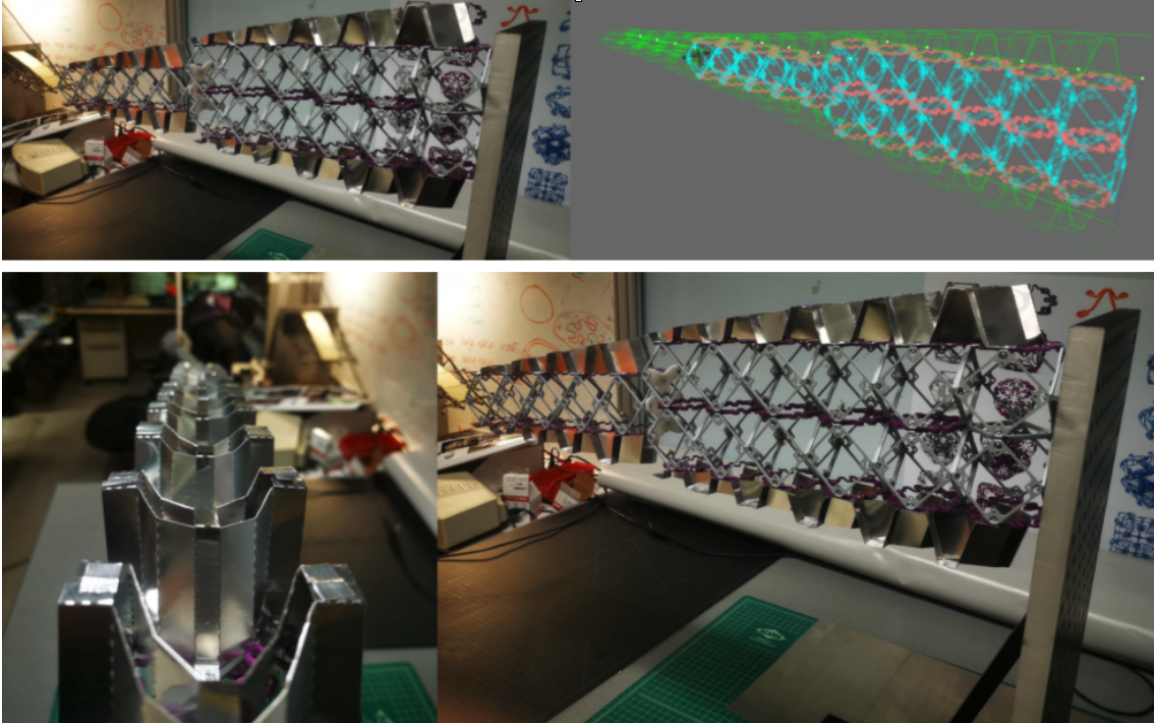


Figure 3-17: Metal folding of a Trailing Edge

out of aluminum.

To fold this composite, I made a 2 faces engraving process milling on each side of the sheet the corresponding peaks or valleys. To manufacture a hinge on a continuum way, the engraving process removes material decreasing locally the bending stiffness and as a result, the material will always want to bend through that area. The benefits of having a thermoplastic as a core are that by milling the top aluminum layer and partially the core, increasing the temperature of the milled piece to the polypropylene glass transition temperature will let us fold it without damaging the core. Once folded, the temperature will cold down, being now at its new position. This thermoplastic core will also help to design specific radii of bending.

Chapter 4

Applications

In this chapter, I show how I use the described and characterized mechanical metamaterial construction kit to develop discrete continuum robots emphasizing their hydrodynamic behavior, simple design workflow, and manufacturing benefits. This thesis finds great interest in aero/hydrodynamics usage of this type of robotic structures as their controlled continuum deformation mimics how nature provides more efficient solutions to generate propulsion or lift. A 1-dimensional robot (morphing beam) and a 2-dimensional robot (morphing surface) serve as examples. For each example, this chapter will describe the design, manufacturing, control, simulations, and water tank testing.

The first showcase is a Hydrosnake robot, a large aspect ratio (1500 mm length and 75 by 75 mm cross-section) discrete beam composed of 4 individual sections serially actuated. This bio-inspired swimming device serves as a platform to show an economical large-scale soft continuum robot with minimal DOF and unique parts.

The second showcase is a camber morphing wing. Alternative methods to maximize the lift-to-drag ratio (L/D) on wings are a high-interest topic in academia. New materials enable alternative bio-inspired strategies to control active lifting surfaces. This second example proposes a non-monolithic solution to generate camber morphing over a 675 mm span wing discretely assembled. Its L/D results are compared with a classic configuration wing to quantify its hydrodynamic benefits.

4.1 Hydrosnake

I had the great help in this project of Ben Jenett, Dixia Fan, Filippos Turlomousis, Jiri Zemanek and Chris Cameron.

4.1.1 Motivation

Unlike traditional engineering solutions for underwater transportation, organism means of locomotion heavily relies on compliant mechanical structures to elegantly overcome environmental constraints very efficiently. As an example, vortical wakes resulting from flow separation affect any submerged body with a certain velocity. For human-engineered creations, this impacts its pressure drag causing a loss of efficiency. On the other hand, fish resonate their flexible body with it and extract energy from those vortices to generate thrust from their own drag.

Replicating this nature-like using a rigid body engineering perspective would generate a hyper redundant complex design. As an example, one of the biggest successes in this premise, RoboTuna, able to replicate swimming physics helping to solve Gray's paradox, was composed of over 3000 unique pieces that collectively interact.

Another type of approach to solve this challenge as continuum robotics or soft robotics can be very size/scale-dependent and generate a 1500mm length robot is a state-of-the-art challenge. Soft robots primarily use elastomeric materials and suffer from scale because the high density of the used rubbers would difficult to hold their own weight [28] [42]. On the other hand, continuum robotics scale problems reside on the complexity of the structures.[7].

This first application shows a novel approach to easily scale up continuum soft robots by combining two unique injection molded parts. The system is able to easily attach discrete serial actuation generating a one-dimensional beam snake-like robot capable to replicate bio-inspired swimming motion. I show the design, manufacturing process, control, experiments, and results of the tow tank campaign test.

4.1.2 Design

As shown in chapter 2 of this thesis, I took as a repeatable segment a beam composed of 5 voxels. A stiff cell followed by four bending heterogeneous voxels.

The voxel pitch is 75mm, its cross-section is 2.1mm by 2.1mm. We attached 4 segments in serial resulting in a robot of 1500mm in length. The mechanical characteristics of this construction can be seen in Chapter 2.

Subsystems were needed to make a snake-like cross-section capable of generating thrust while swimming. Skinning the snake is a key point of the project as having a smooth tangent surface without fabric wrinkles is key to drop down from drag. It was achieved by making a hierarchical overlapping rib system using 1/32" thickness laser cut Delrin sheets and riveted to the morphing beam module as it can be seen in Fig. 4-1.

The fabric used for the outer skin is composed 94% of polyester and 6% spandex. The system is built by assembling the voxels, implementing servos and tendons, riveting the skin and sliding the built skeleton inside the elastic skin.

4.1.3 Control

Our target was to replicate the swimming shapes that a fish body generates as a continuous system. There is research work on describing mathematically the kinematics and dynamics of traveling-wave-like propulsion systems of anguilliform swim strategies [26].

$$y(x, t) = \frac{A_t}{1 - e^{\alpha L}}(1 - e^{-\alpha x})\sin\left(\frac{2\pi}{\lambda}x - 2\pi ft\right)$$

Where $y(x, t)$ is the y coordinate position as a function of x and the current time. L corresponds to the length of the robot (1.5m), A_t is the amplitude of the tail motion. We choose it to be a relation of the length, iterating from 0.15L to 0.35L. At the tow tank, we decided to test from 0.15 Hz to 0.25 Hz. Finally, α controls the conical shape in which the amplitude grows from the leading edge to the trailing edge of the robot. The tested value corresponds with $\alpha = 1.5$.

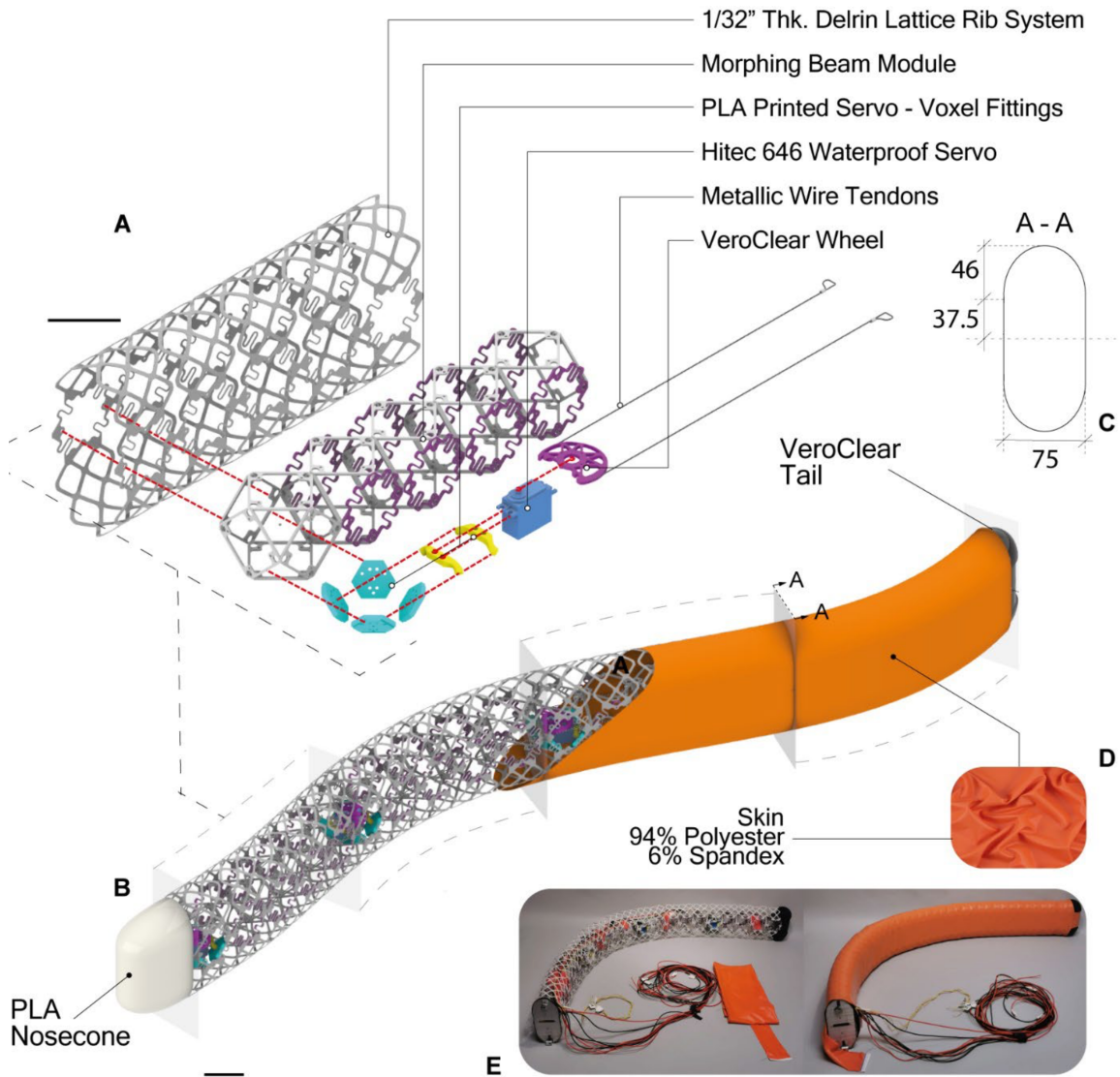


Figure 4-1: Aquatic discrete cellular soft robot system architecture. A) Exploded-View of a section. The robot is composed of 4 of these elements in series. B) Isometric view of the robot highlighting main parts. C) Cross section drawing. D) Texture of the skin fabric. E) Prototyped robot with and without skin. Scales: A) 75mm B) 75mm

With 4 continuum radius sections, we were able to match an acceptable accuracy on the ideal traveling-wave spline as it can be in figure 4-2.

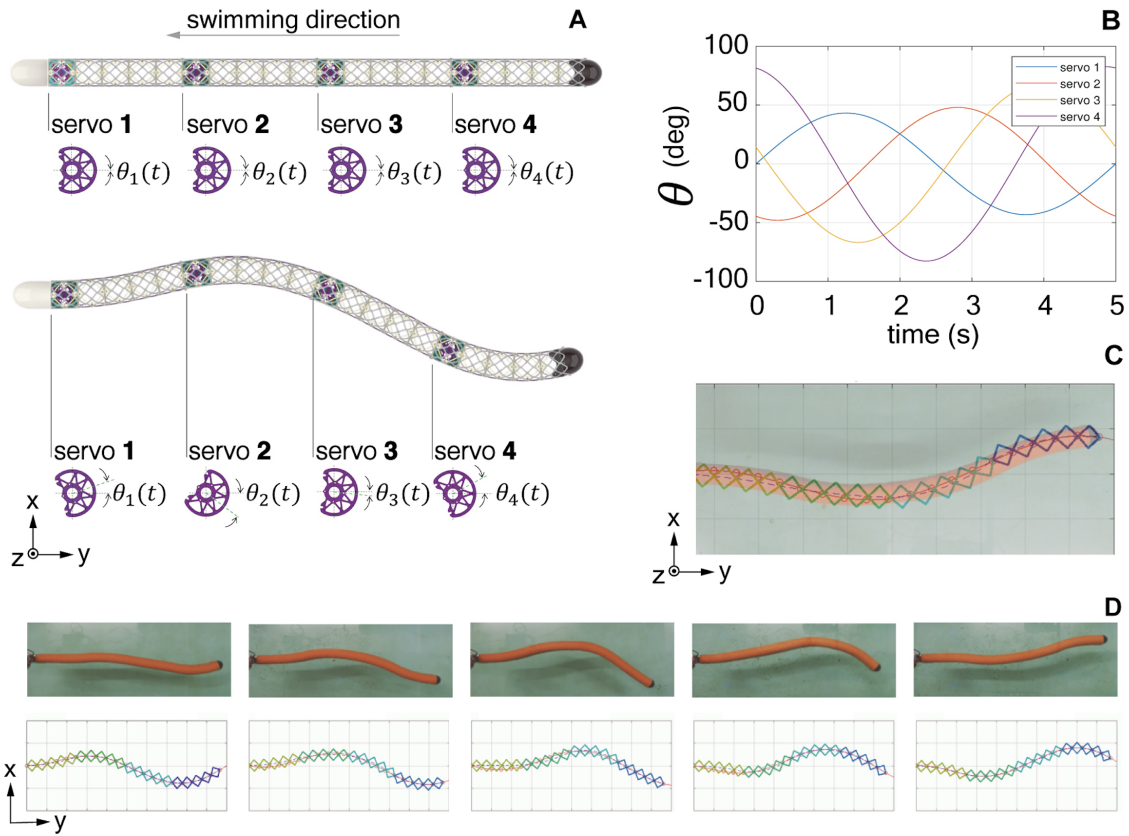


Figure 4-2: Section-composition of the swimming robot. A. Continuum curvature sections in series replicates target splines. B. Servo actuation phases over time. C. Matching simulation with actuation in a quasi static state. D. Dynamic matching.

4.1.4 Results

Tow Tank Setup

The hydrodynamics of the bio-inspired discrete cellular soft robot were tested at the MIT Towing Tank facility, which features a 33.3 m x 2.67 m x 1.33 m testing tank section and a belt-driven carriage able to achieve steady linear motion at speeds from $U = 0.05$ m/s to 2.3 m/s. The robot is connected to an ATI underwater gamma load cell (Item 6 in Fig. 4-3) that is linked to an 8020 aluminum strut (Item 5 in Fig. 4-4, and the size of its cross-section is 7.62cm x 3.81cm) and then is mounted at the front of the carriage (Item 2 in Fig. 4-3) as shown in Fig. 4-3. The power, control, and data acquisition system (Item 1 in Fig. 4-3) includes an Arduino Mega microcontroller for robot motion control, an ATI gamma load cell amplifier and NI

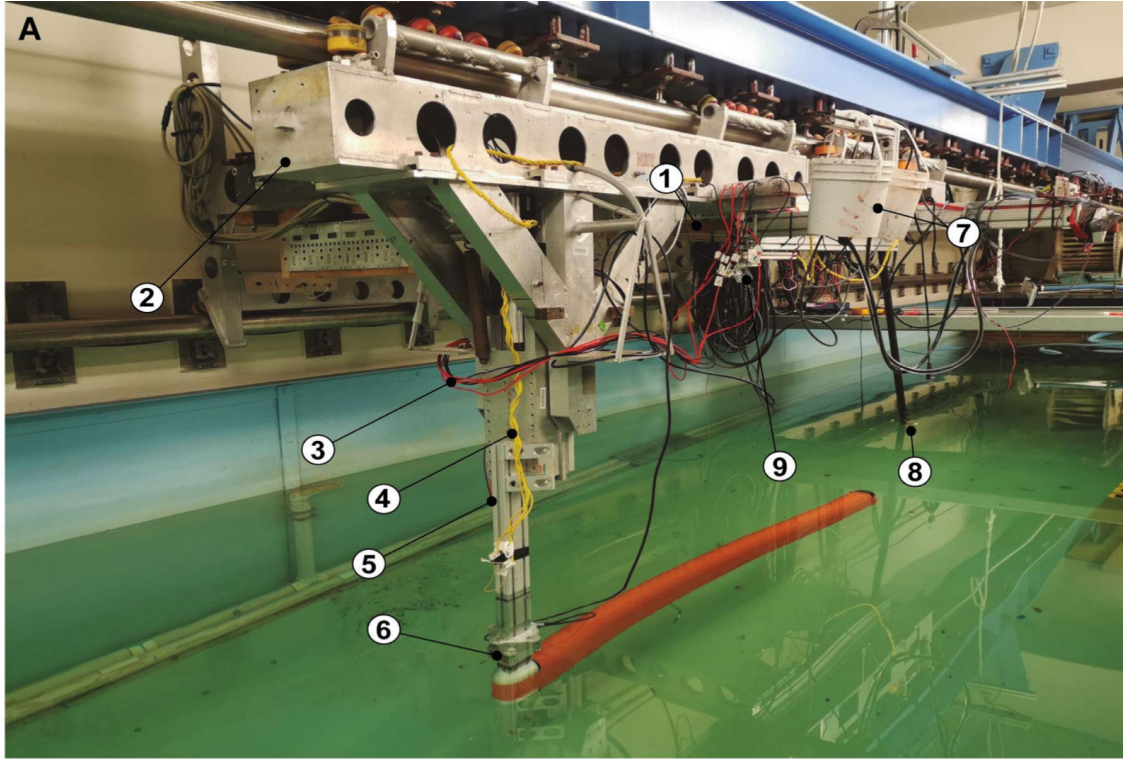


Figure 4-3: Tow tank experiment setup. A) 1. Control center zone. Dell computer, Arduino mega microcontroller, ATI gamma load cell amplifier, NI USB-6218 DAQ board and power supplies. 2. Tow tank carriage. 3. Power lines from fuses to servos. 4. Signal lines from microcontroller to servos. 5. Snake - Carrier fitting. 6. Load Cell. 7. Ink system. 8. Water lights. 9. Camera. B) Snapshot from the camera point of view. C) Complete track of the tow tank. D) Detailed design of the carrier - snake fitting. 1) Aluminum 1/4' waterjet sheets.

USB-6218 data acquisition (DAQ) system for force measurement, a power supply and a Dell computer for data logging via LabVIEW, mounted on top of the towing carriage and remotely accessed during the experiment. In addition, three 1500 lumen underwater lights (Item 8 in Fig. 6) are placed in the 1.5m back from the tail of the model, providing sufficiently strong background lighting for the camera (Item 9 in Fig. 4-3) to capture the robot motion in the water as well as the wake pattern visualized by the dye injection system (Item 7 in Fig. 4-3). Note that to avoid model sagging and excessive torque on the load cell due to the robot weight, distributed buoyancy modules are inserted inside the voxel, making the robot neutrally buoyant. Thanks to the small size and location of the buoyancy modules, their existence has minimal

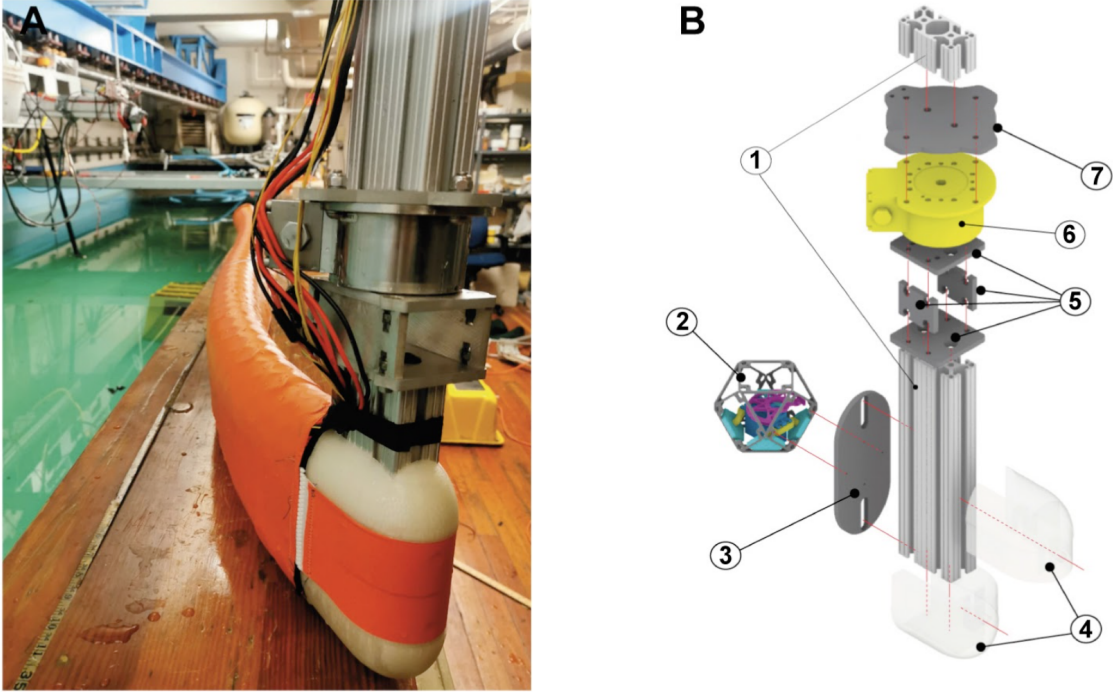


Figure 4-4: Robot - Carriage Assembly System A) Prototype ready to go to the water. B) Exploded view of the current design. (1) 8020 1530 aluminum beam. (2) First voxel of the robot. (3) 1/4" waterjet aluminum plate. (4) PLA 3d printed leading edge. (5) Lower fitting. 1/4" waterjet aluminum plate. (6) ATI Gamma Sensor IP68. (7) Upper fitting. 1/4" waterjet aluminum plate.

effects on the dynamics or hydrodynamics of the robot during the experiment.

Tank Results

The model was towed at a constant speed U of 0.1 m/s but iterating over λ and α values. The ATI gamma load cell measured the force at a sampling rate of 1000 Hz. The end goal was to prove thrust generation and to do so, we measured non-dimensional thrust coefficient C_t defined as:

$$C_t = \frac{F_x}{0.5\rho U^2 S_w}$$

Where F_x is the average force in the towed direction from tail to head, ρ is the water density, and S_w is the wet surface of the robot with a value of 0.6138 m^2

The thrust coefficient C_T of the robot being towed at $U = 0.1\text{m/s}$ (Reynolds

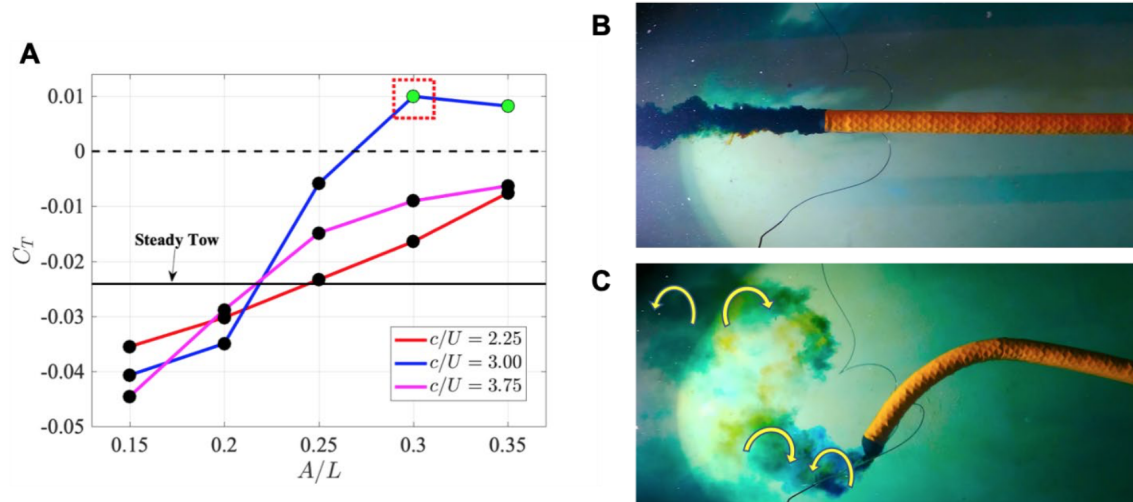


Figure 4-5: The result of the hydrodynamic experiment of the robot being towed at $U = 0.1$ m/s. A) The thrust coefficient C_t vs. commanded $\frac{A}{L}$ for various $\frac{c}{U}$ ($\lambda = L = 1.5$ m). B) The wake pattern of the unactuated robot, represented by the in black solid line in subfigure A. C) The wake pattern of the actuated robot with $\frac{c}{U} = 3$, $A_t = 0.3L = 0.45$ m and $\lambda = L = 1.5$ m, highlighted by the in dotted red box in the subfigure A. Negative C_t (black dots) are the average drag force on the robot, while positive C_t (green dots) indicates the average thrust force produced by the robot.

number $Re = \frac{UL}{\nu} = 150,000$ where ν is the kinematic viscosity of the water) is plotted in figure 4-5. The thrust coefficient of the unactuated robot is $C_T = -0.0248$ (highlighted as the solid black line in Fig. 4-5). At a fixed $\lambda = L$, C_T increase with tail amplitude

As it can be seen in Fig. 4-5, with values of $\frac{A}{L}$ higher than 0.25 the dynamic traveling wave decreases the overall drag of the robot, being able to generate thrust for values of $\frac{A}{L}$ higher than 0.3.

4.2 Camber Morphing Wing

I had the great help in this project of David Preiss on stepper motor actuation, Dixia Fan and José del Águila Ferrandis for simulation and Jill Marie Uzoma with tow tank testing and data management.

4.2.1 Motivation

The need for control surfaces with a smooth and continuum deformation was known since the Wright Brothers took inspiration from birds to build the first heavier-than-air powered aircraft. They implemented a warping morphing wing (continuum change of the angle of attack along the span) to achieve lateral stability the same way birds do. The Flyer 1 was mainly built of wood and dry fabrics actuated by steel tendons[37].

As aviation advanced, engineers and designers realized that increasing the power of the engine would help to maximize the trade-off between payload, endurance, and range. That resulted in the need of using very stiff and, where possible, light materials as loads become inaccessible for wood and dry fabrics [45].

The tendency keeps until nowadays where almost any aeronautical structure is a redundant rigid body design comprising links and rotations. This thesis studies as a base technology in which bio-inspired wing designs could overcome the technical difficulties that monolithic rigid configurations are currently facing. This second application shows a wing design build upon an ultra-light discrete lattice with controlled mechanical anisotropies in which a camber morphing is used with two proposes:

1. - became a different member of the airfoil family in different flight regime. That is break its intrinsic symmetry.
2. - use the morphing as an elevator/aileron for flight stability/control.

Optimizing the performance of flight control surfaces is a crowded research question and morphing is an attractive solution. Flight conditions change constantly and ideally, wing shapes should do the same, adapting to behave optimally for those different regimes. Cruise conditions, maneuvering, slow-speed approach conditions require drastically different morphologies. Offering a system able to morph accordingly while holding loads could help to improve aviation's environmental performance, saving billions of fuel gallons yearly and reducing millions of CO_2 tons [30].

Different morphing strategies for flight control surfaces have been offered as the Morphing Wiglet by the European consortium Clean Sky [44] [12]. But their approach

only focused on morphing with classic mechanical assemblies the wingtip for end-vortex reduction.

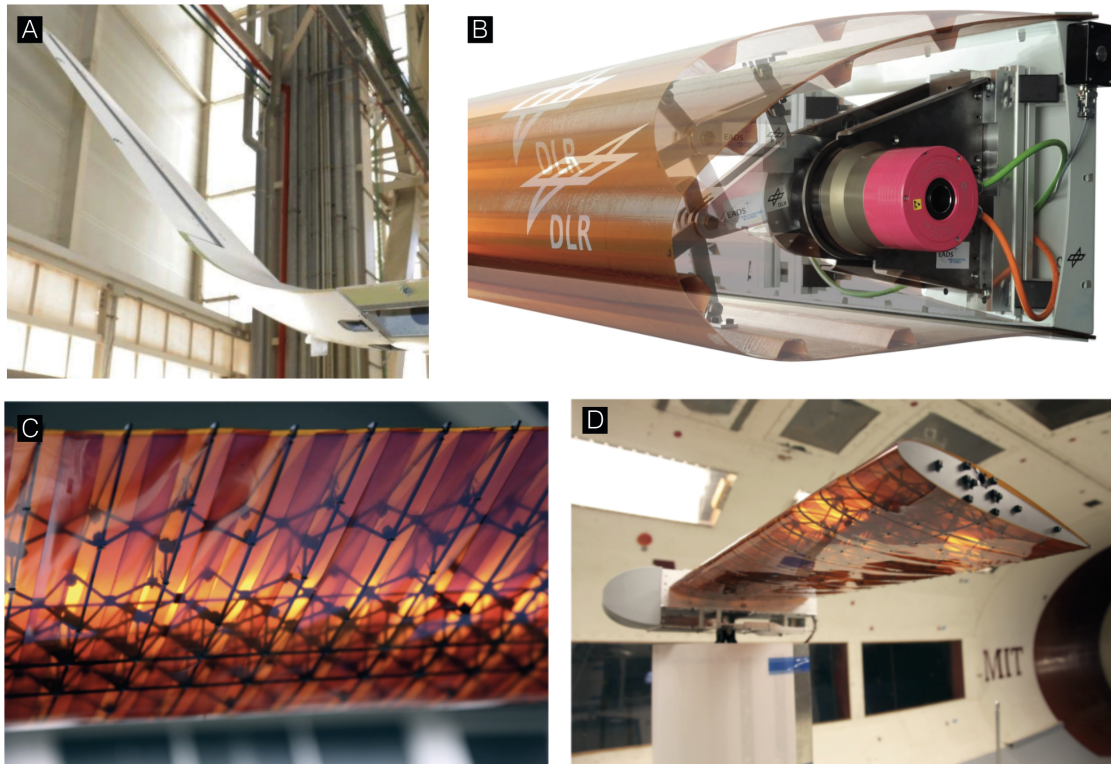


Figure 4-6: Morphing examples. A) FACC Active Morphing. B) DLR leading edge. C) and D) NASA-CBA Digital Morphing Wing.

The German aerospace center DLR offered a full research roadmap on adaptive wing technologies. Their more interesting proposal was an actively actuated leading edge, being able to find drag reductions for angles of attack between 5 and -5 degrees [43]. There still be a challenge for this technology to propose control surfaces.

A digital wing by the CBA was researched offering a lattice-based structure able to perform spanwise twist deformations [?]. They used an inspired Kelvin lattice shape to generate a torsion box compliant on its twist along the span, controlled by a single DOF. This approach maintains the same airfoil cross-section and has a high interest for stability proposes but not for control or flight optimization.

In this subsection of Chapter 4, I revisit a different approach to build and provide an out-of-plane morphing of a torsion box. Instead of proposing a light design with

maximum bending stiffness at its cross-section along the span, I use a heterogeneous lattice surface to build a camber morphing wing. I simulate and test the lift-to-drag ratio that is achieved by actuating the camber line of an airfoil and compare with a classical rotation along its aerodynamic center. To show its performance compared to a classic wing configuration, I build a semi-monocoque rigid wing out of a custom modified Eppler profile and test it at the Sea Grant MIT Tow Tank at different angles of attack to measure aerodynamic performance. Then I build a twin but out of heterogeneous digital materials able to morph and do performance tests at different angles of attack and tail deflections. We compare L/D performances, meaning, at which cost of drag I achieve a unit of lift.

This technology opens the possibility to generate wings that locally their cross-sections could become unique members of the foil family as desired in different flight regimes. Also, it can be used as a flight control surface, potentially reducing movable systems as tip-ailerons.

4.2.2 Design

While the first example shown in this chapter is a one-dimensional robot, similar to continuum robotics models, this second concept wants to demonstrate the dimensional addition we can easily create with this building block kit. Here we are proposing a morphable surface. We are using a heterogeneous surface by adding 9 heterogeneous beams along the span of the wing. The resultant surface will be a torsion box with a very low value of bending stiffness along the cord. That gives us the possibility of generating a camber morphing foil.

First I designed a modification of an Eppler 838 using XFLR5 as can be seen in Fig. [?]. I increased the thickness close to the trailing edge to delay the boundary layer separation at a high angle of attack but also to make fit an array of 4 voxels inside the wing without becoming too large to test at the tow tank.

I started building a rigid classic semi-monocoque wing using that profile. The span of it will be the corresponding with 9 layers of voxels for future comparison. Drawings for this design are shown in Fig. ??.

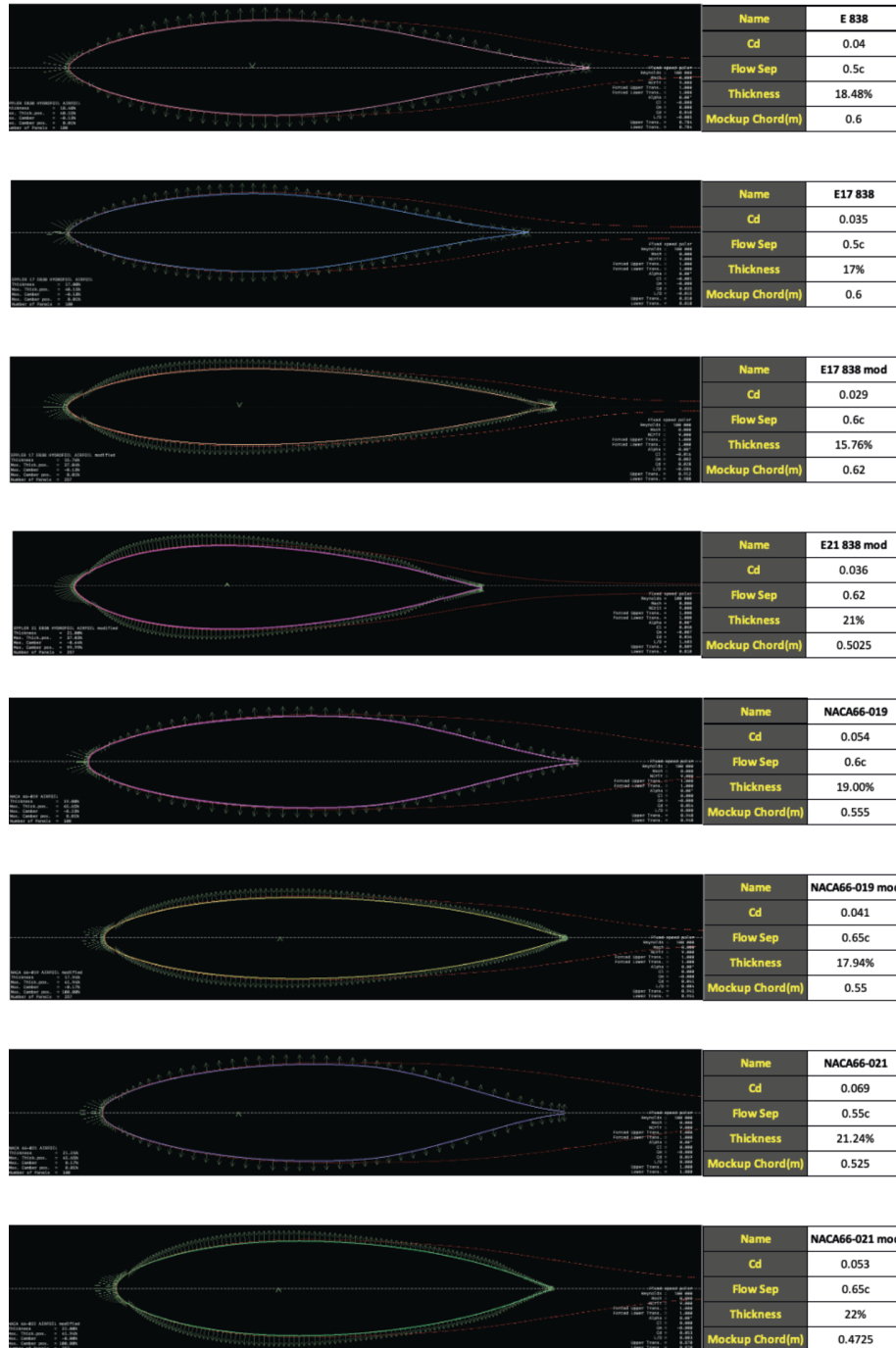


Figure 4-7: Eppler and Naca candidates to design a hydrofoil.

Second, I started designing the camber morphing wing. I propose a compliant cross-section composed of 3 main parts as can be seen in Fig. 4-10. The first section, the segment from A to B will be a rigid leading edge, where I locate the cantilever beam to hold the wing to the load cell and the stepper motor embedded in a stiff

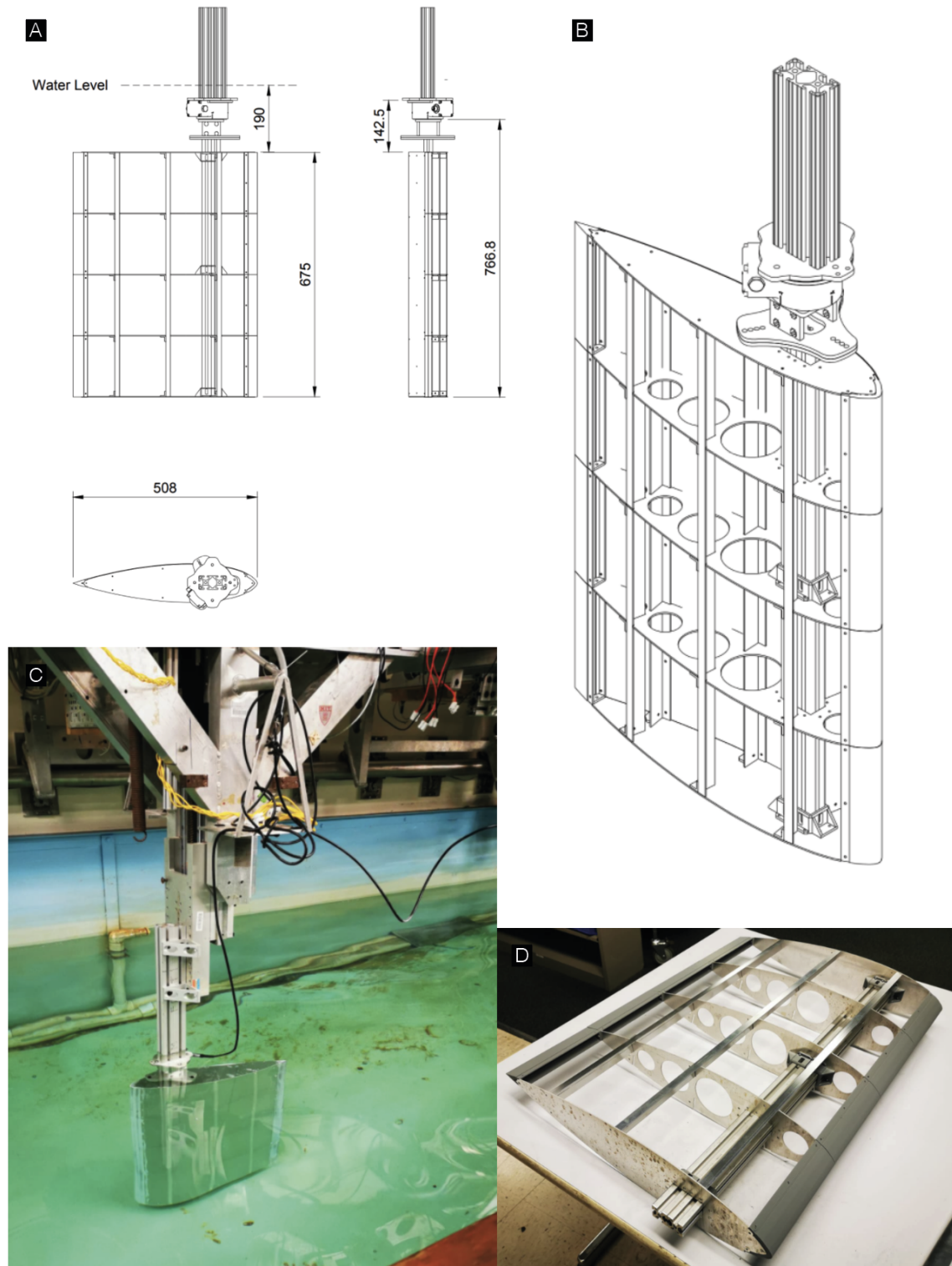


Figure 4-8: Digital morphing wing system architecture. A) Exploded isometric view of a wing section. Scale 75mm. B) Isometric view of the full assembly. Scale 75mm.

voxel. A second segment from B to C in which the morph will occur. This segment is the heterogeneous lattice section. Finally, a third rigid trailing edge, from C to D, in which the dynamic pressure will reach maximum values.

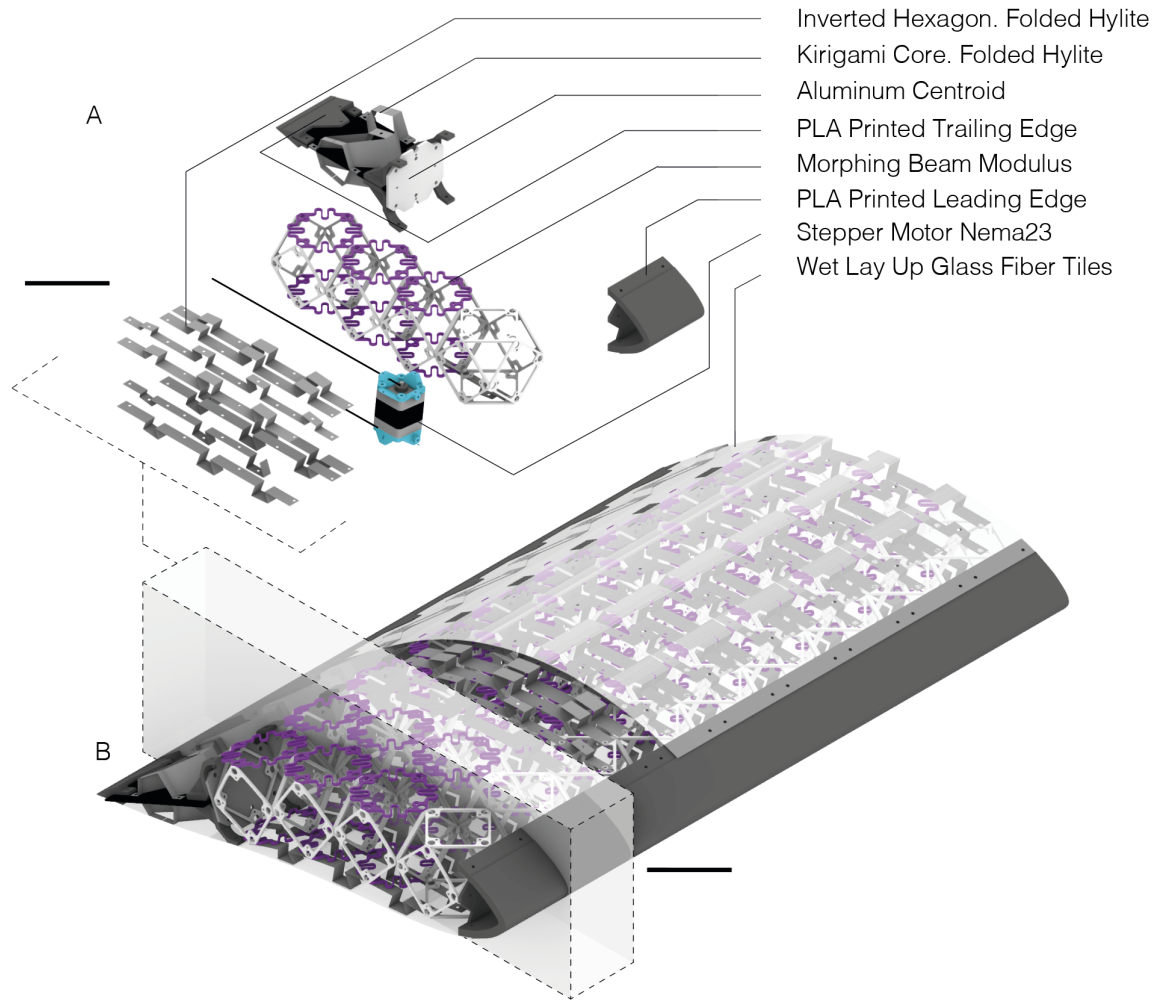


Figure 4-9: Digital morphing wing system architecture. A) Exploded isometric view of a wing section. Scale 75mm. B) Isometric view of the full assembly. Scale 75mm.

We need to specify the characteristic angles of this approach. . On the one hand, we call the angle of attack α to the angle of rotation of the full-body around the axis of its aerodynamic center. On the other hand, we call tail angle θ at the one generated by morphing the wing as it can be seen in Fig. 4-10

For control and simulation proposes, I determined the equations of this centroid-based morphing based on the conclusions extracted from Chapter 2, in which we could

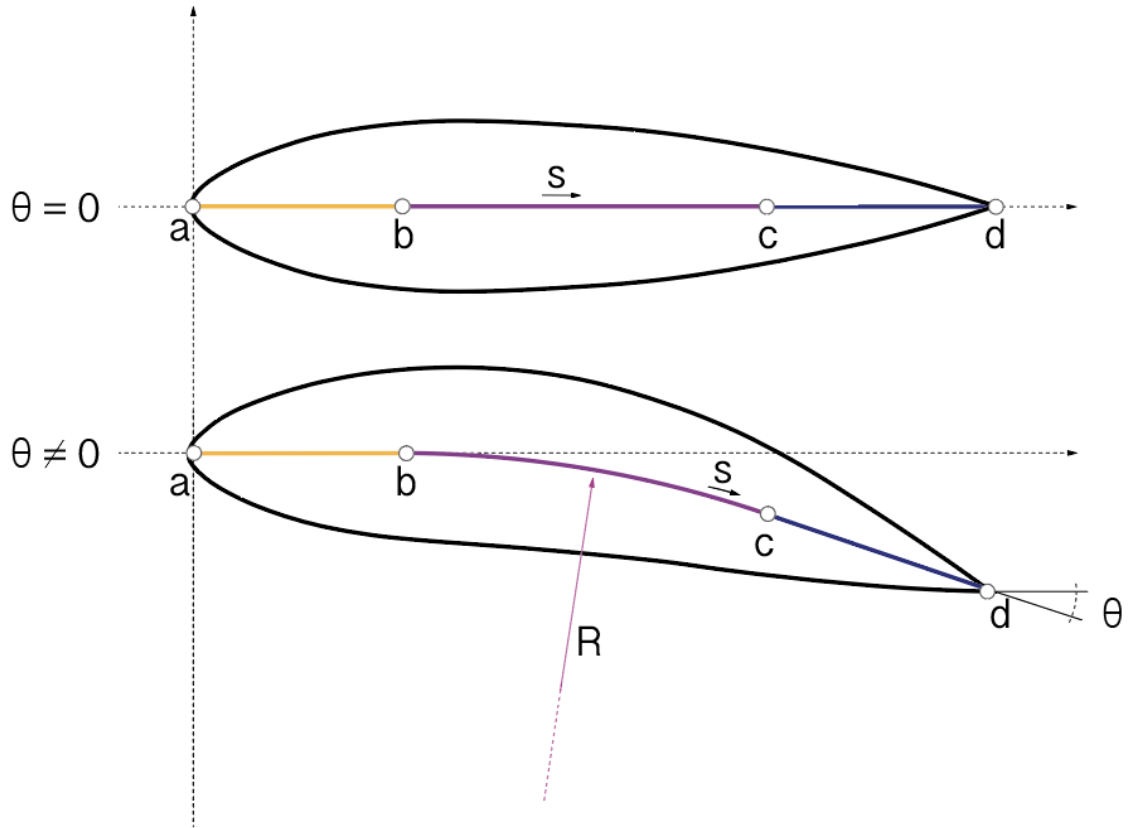


Figure 4-10: Centroid-based characterization of morphing.

assume constant curvature deflections for tendon actuated foams. Given a point of the centroid $p \in R^2$ we obtain its x and y coordinates given an evaluated length s of that spline. We see that those x and y coordinates will be a function of the evaluated length and the tail angle, $p(s, \theta)$. To calculate the position in any evaluated length, we can follow:

$$p(s, \theta) = \begin{cases} \begin{cases} x = s \\ y = 0 \end{cases} & \text{for } s \in [a, b) \\ \begin{cases} x = \frac{c-b}{\theta} \sin(\theta \frac{s-b}{c-b}) + b \\ y = \frac{c-b}{\theta} \cos(\theta \frac{s-b}{c-b}) - 1 \end{cases} & \text{for } s \in [b, c) \\ \begin{cases} x = -\sin(\theta - \frac{\pi}{2})(s - c) + \frac{c-b}{\theta} \sin(\theta) + b \\ y = -\cos(\theta - \frac{\pi}{2})(s - c) + \frac{c-b}{\theta} (\cos(\theta) - 1) \end{cases} & \text{for } s \in [c, d] \end{cases} \quad (4.1)$$

With this system we can calculate any spline shape at any angle, and tracing normals along its spline we can determine the shape of the airfoil given any tail angle θ . Implementing this analytical forming in Rhino-Grasshopper we obtain:

The adaptation to the outer mold line was done as Chapter 3 shows. I design a inverted semi hexagon shape for the zones in which I need to respect the anisotropies, offering structural integrity but bending compliance. For the rigid tail, I used a negative slope cell.

I designed pre-stressed tiles skin able to slide between them while always working on compression on specific zones of the inverted hexagon.

4.2.3 Actuation Control

With the Hydrosnake we learned that it is crucial to hold torque on this structure without increasing the power consumption of your actuator. Many times we would stall the servo resulting in burning them inside water. That is why we change here

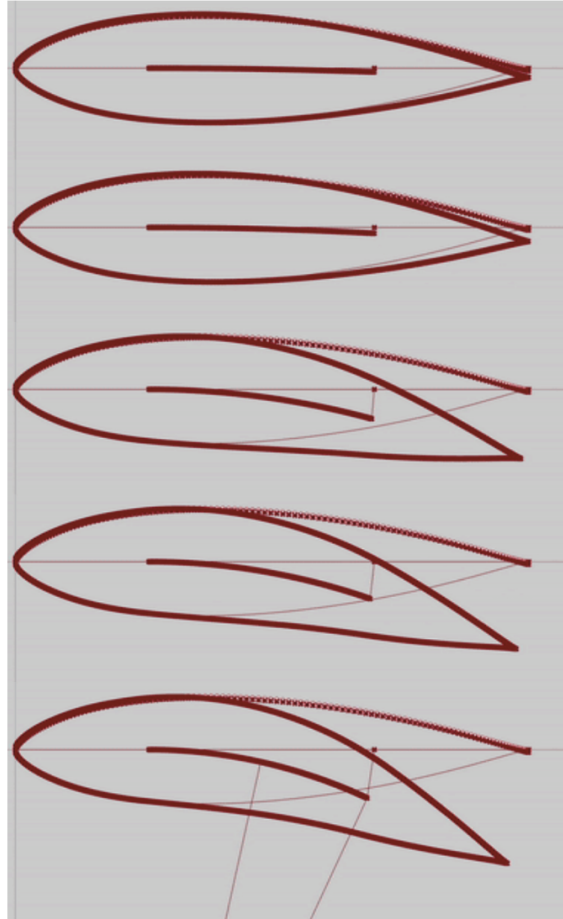


Figure 4-11: Geometry solutions for the centroid based method.

from high torque waterproof servos to stepper motors. Dual shaft Nema23 enables the possibility if placed correctly, to pull bidirectionally a heterogeneous beam. Also, they hold torque at no power consumption increase and that is ideal for this goal.

After fast XFLR5 simulations of pressure distribution at different angles of attack and tail angles, I choose a worst-case scenario to dimensionalize the required torque for the actuation platform. The result was that with 3 stepper motors Nema23 was able to hold up to 1.3 Nm.

The stepper will be assembled inside the first layer of rigid voxels, pulling tendons to an aluminum frame that encapsulates the whole heterogeneous construction. A system to individually pre-stress the tendons was needed to guarantee that backlash won't affect the performance.

When installed, the wing is able to perform up to 12.5 angles of rotation contin-

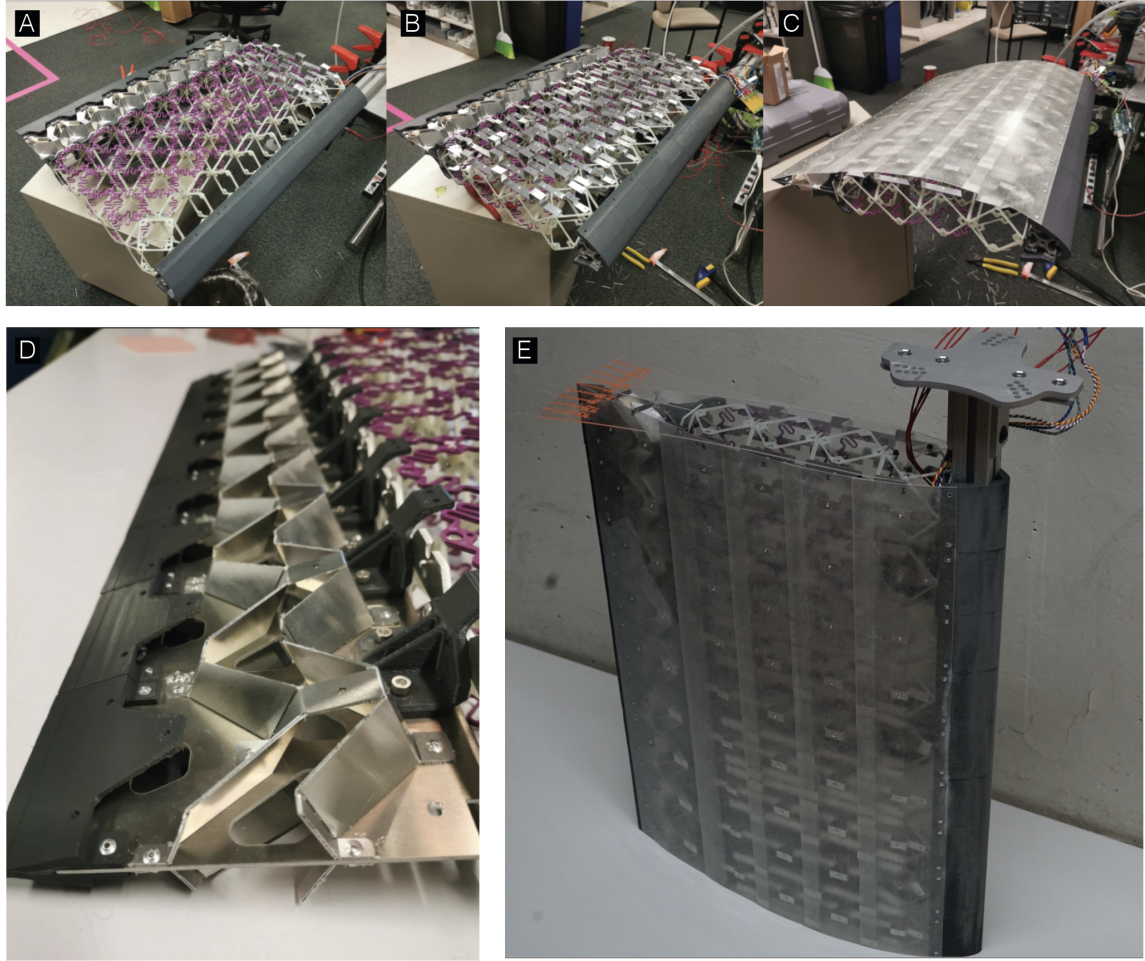


Figure 4-12: A) Voxel torsion box. B) Adding inverted hexagon. C) Adding glass fiber skin. D) Positive slope origami cell. E) Complete assembly before the test.

uously as Fig. 4-13 shows.

4.2.4 Simulations

First, we obtain the pressure distribution of the wing using XFLR5 for the worst-case scenario, an angle of attack α of 12.5deg with a tail deflection θ of 12.5deg.

A structural simulation using Oasys GSA was done implementing the obtained pressure distribution with a strain in the opposite direction provided by the tendon actuation. Fig. 4-14 shows that the residual tension of the tendon reached 100N. In conclusion, we could govern the behavior of this three sections with one Nema23, thus, for the whole wing we can use only 3 motors.

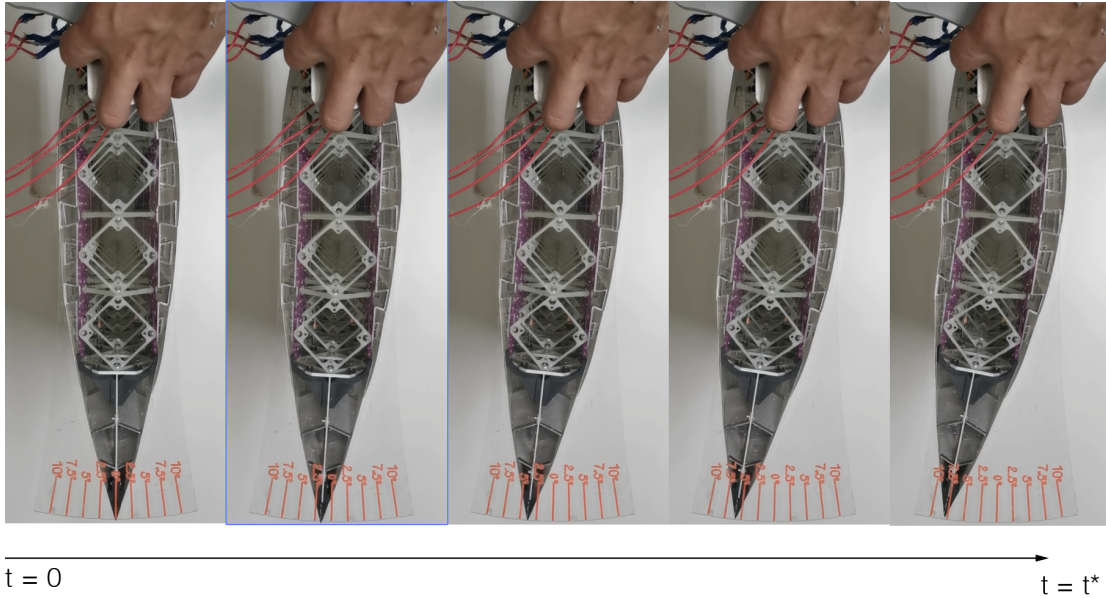


Figure 4-13: Frames of the actuators morphing the wing.

4.2.5 Tow Tank Setup

Same procedure as in the Hydrosnake was follow to install the wing inside the tow tank.

4.2.6 Results

We performed the test under the same configuration as the Hydrosnake. Details of the tow tank and measurement devices are shown in Chapter 4.

The water temperature is $22^{\circ}C$, and that sets the value for Kinematic Viscosity at $9.554 \frac{m^2}{s}$. Given that the chord is $507mm$ for both wings and the towing velocity is $0.2ms$, we will compare results performing at a Reynolds number $Re = 106134$.

The mounting bracket, that joins the wing (fix and morphing) to the load cell, allows us to generate deltas on the wing's angle of attack by 2.5 degrees. Thus, the experiment matrix for the morphing wing will be the one corresponding with Table 4.1.

Results for the rigid wing are shown in Fig. 4-16

This thesis characterizes the morphed shapes by the tangent angle that the tail

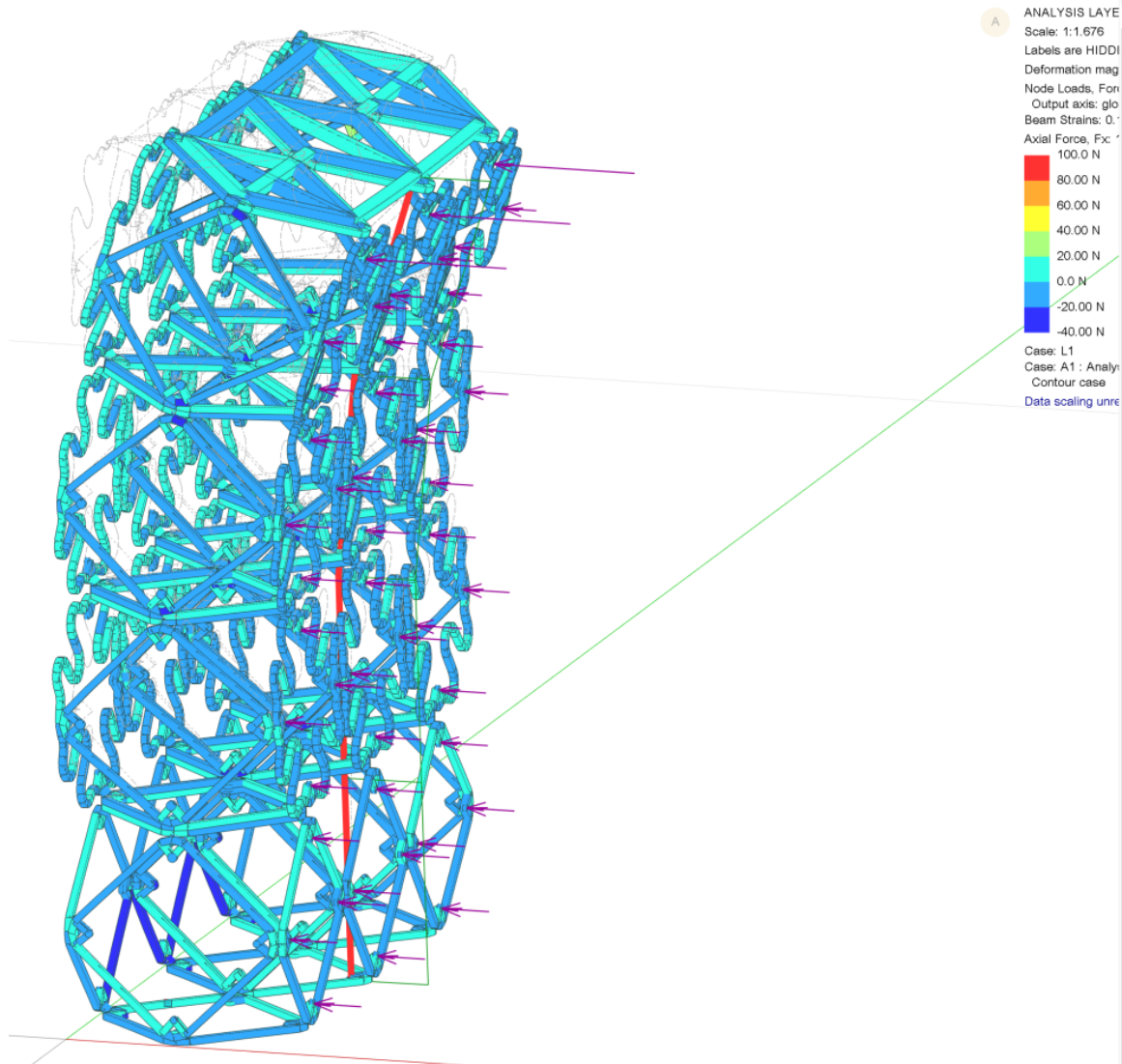


Figure 4-14: Oasis GSA axial stresses for 1/3 of the wing section.

forms with the free streamline direction. We perform now, for every angle of attack, 6 more experiments with different tail angles, from 0 to 12.5 in steps of 2.5 degrees.

Aerodynamically, what we are doing is making the original airfoil Eppler22 become a new member of the family. As we are increasing the curvature of the centerline, by breaking the symmetry of the foil, we can generate different L/D coefficients.

This study doesn't consider comparisons with main control surfaces as it can be an aileron, flaps, or a spoiler. Morphing should be treated in this case as a change in the overall airfoil morphology, not a device to control a fixed foil. That is why this result compares, for every L/D value of the rigid wing at different AoA, how does

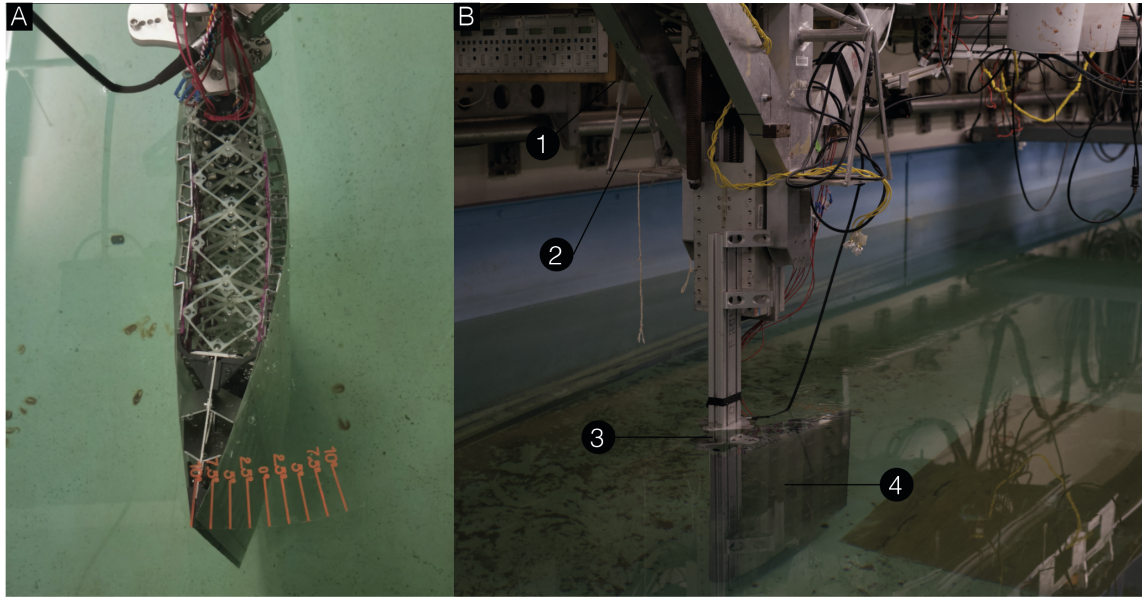


Figure 4-15: A). Wing in the water at $\theta = 10$ deg. B) 1. Control station (not visible, beneath the gantry). Power supply, microcontroller, computer, stepper drivers and cooling station. 2. Towing carriage. 3. 6 axis load cell. 4. Wing

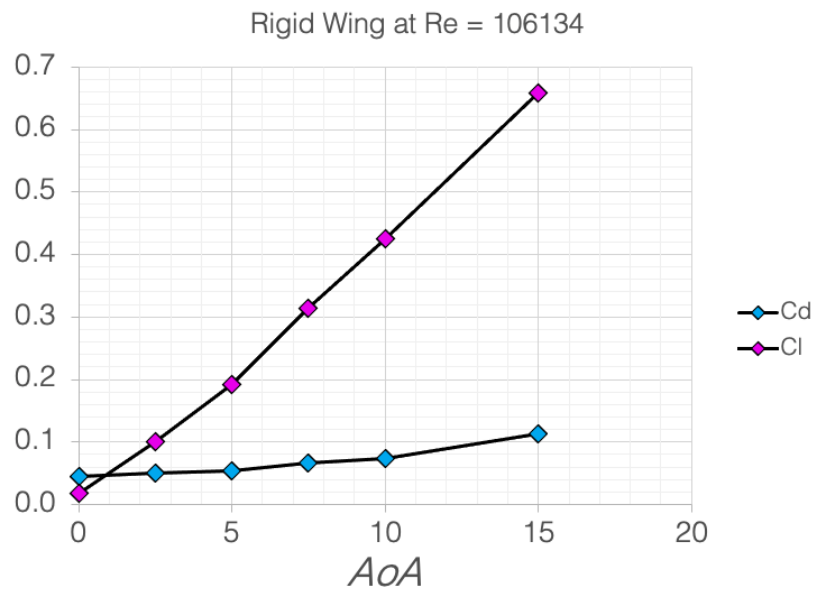


Figure 4-16: Cd and Cl values vs. Angle of Attack.

this factor changes with different morphed shapes, characterized in this study as tail angles.

We can see that we drastically increase the L/D performance of the rigid wing by providing curvature to the chord. It can be seen how, speaking just in terms of

Sample	AoA
1	0
2	0
3	2.5
4	2.5
5	5
6	5
7	7.5
8	7.5
9	10
10	10
11	15
12	15

Table 4.1: Test number with its corresponding AoA

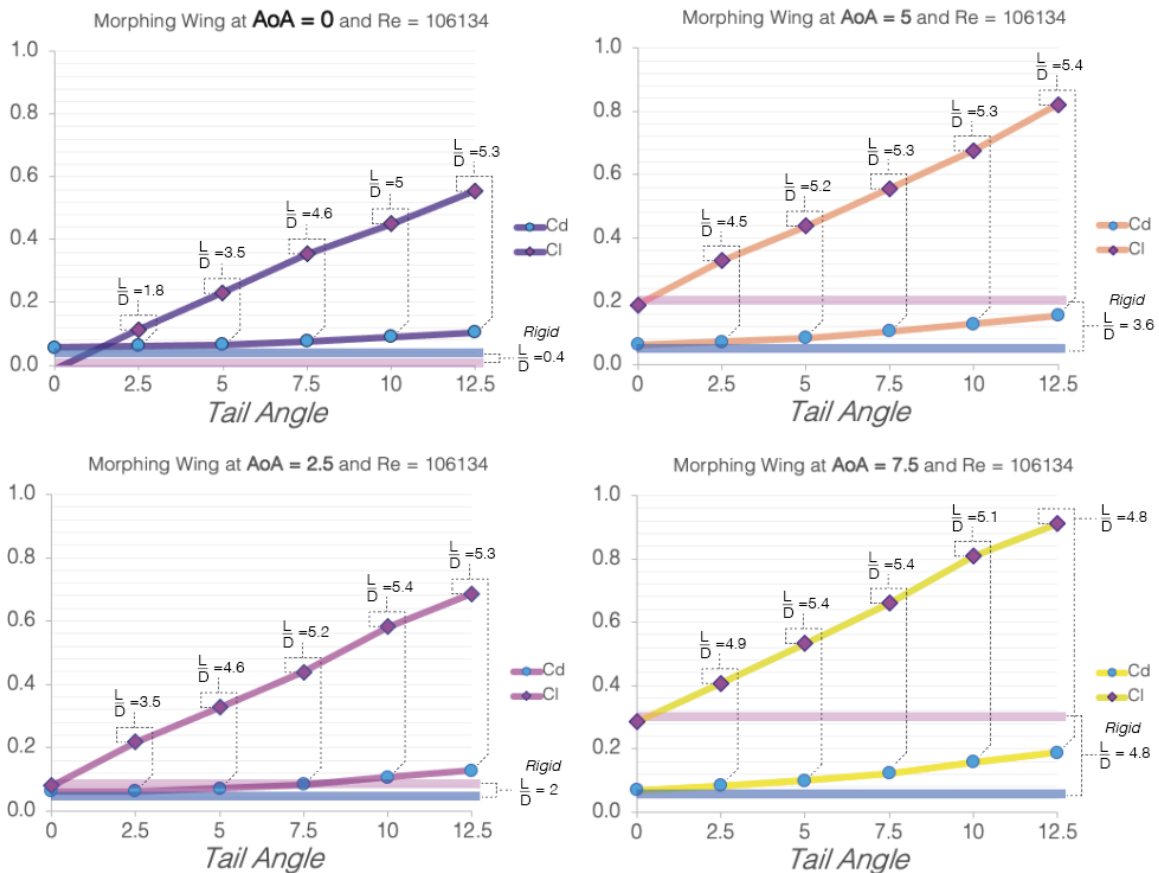


Figure 4-17: Cd and Cl values vs. Tail Angles for every Angle of Attack (AoA). In every plot, the pink horizontal line corresponds with the cl value of the rigid version and the blue horizontal line represents the cd of the rigid wing.

maximum values, for the same angle of attack we can increase the cl coefficient by a 320% while increasing its cd a 250 %. As in the graphs, we don't appreciate a drastic decrease of L/D values, we can set that we are not having yet flow separation. Further results at higher speeds will be done to characterize this behavior.

To have a sense of performance with all the variables involved, we show in Fig. 4-18 a contour map of all the variables involved in this experiment. In the X-axis we show the Angles of Attack, in the y axis Tail Angle values and its corresponding L/D as Z-colored information to make a heat map.

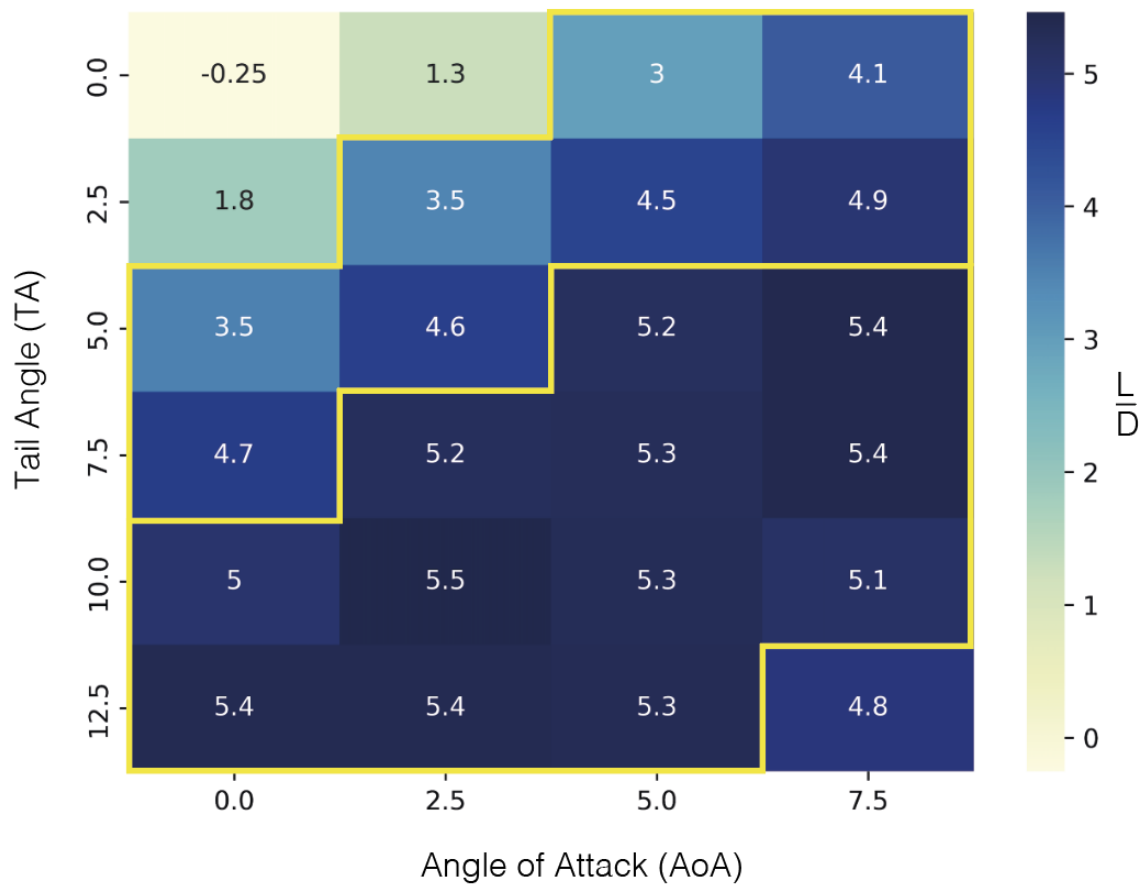


Figure 4-18: Contour map for L/D values given an AoA and a Tail Angle. Yellow lines sets zones for L/D higher than 3 and 5

Fig. 4-18 shows where the point of maximum performance was found, corresponding with $AoA = 2.5$ and $TA = 10$. Also, we can see the improvement of the morphing over fixed AoA, where the maximum delta can be found at $AoA = 0$, able to vary

L/D from 0 to 5.4.

Chapter 5

Conclusions

I started this thesis showing intentions to show an alternative to rigid joints and links mechanical assemblies by leaning towards continuum macroscopic foams with controlled heterogeneous mechanical properties. I continued by characterizing the mechanisms we can generate, showing tension - deformation of the preferred axes. Then, I showed an algorithmic method to implement custom outer mold lines for these cellular metamaterials and I finished by showing macroscopic examples of actively actuated morphing structures. In this chapter, I reflect on the result obtained and the path that this research has been.

5.1 Scalability

This thesis shows the tools developed to rapidly built and actuate large-scale soft robotics which is a challenge the field has been founding. While keep relying on elastic deformation to generate motion, the ultra-low relative density of this material system allows scaling much higher. Also, the digital perspective of the material allows the user to design much rapidly as the building axioms remain much simpler than the classic-mechanical-monolithic world. We were able to rapidly develop a 1500mm length robot with less than 200 parts and 20 different parts. As a comparison, RoboTuna was composed of over 3000 unique parts.

5.2 Actuation

This thesis detected as a challenge in the structure that the lack of centroid the same way classic continuum robots have. To have an element working effectively in pure compression would allow a much easier form-finding of the mechanisms as well as a much reliable simulation results.

At the beginning of the project, we used high-torque servomotors but we rapidly detected that holding torque was more important for us than apply torque. That is why we change to stepper motors as, in a 75mm pitch voxel we can fit up to a Nema 23 size of a dual shaft version. That not only gives us a lot of torque but more control and hold torque without power cost.

As a work for the future, it will be very interesting to study if continuum actuation could over-perform our actual solution in terms of simplicity. It would be very interesting as our degrees of freedom would become infinite but might be challenging in terms of system integration, control and power.

5.3 Simulation

Unlike classic rigid robotic structures in which you can determine motion geometrically and capabilities solving FEM, this method blends both onto a single FEM calculation. That is a challenge as truss lattices forces to use non-linear solvers. Calculating the tension of tendon elements increases the difficulty to determine which is the desirable actuation platform. To virtually actuate the structure, pre-stressed elements ought to be launched as load conditions and that is not as accurate as we would like.

Tip displacements are neither a solution, as the displacement is the unknown we want to solve, not to impose.

Friction effects are also neglected in this method but their effect might be non-negligible for certain usages or tension values.

5.4 Design

It is an interesting exercise to design using this platform. As it offers basic axioms to generate specified motion, the design process gets very simplified, showing big potential for educational platforms or design perspectives in the forms of building blocks as many gaming platforms use, but for real robotic structures.

A challenge in the design itself of these structures is the lack of centroid. Future steps will involve providing a facet that reinforces the desired centroid to avoid overall compressibility issues we have found when using pulling actuators as tendons or rods.

Bibliography

- [1] Boston dynamics, <https://www.bostondynamics.com/aboutq1>.
- [2] L. Ai and X.-L. Gao. Metamaterials with negative poisson's ratio and non-positive thermal expansion. *Composite Structures*, 162:70–84, 2017.
- [3] D. N. BEAL, F. S. HOVER, M. S. TRIANTAFYLLOU, J. C. LIAO, and G. V. LAUDER. Passive propulsion in vortex wakes. *Journal of Fluid Mechanics*, 549:385–402, 2006.
- [4] J. Benyus. Biomimicry: Innovation inspired by nature. 1997.
- [5] G. Bledt, Matthew J. Powell, B. Katz, J. Carlo, P. Wensing, and Sangbae Kim. Mit cheetah 3: Design and control of a robust, dynamic quadruped robot. *2018 IEEE/RSJ International Conference on Intelligent Robots and Systems (IROS)*, pages 2245–2252, 2018.
- [6] Elisa Boatti, Nikolaos Vasios, and Katia Bertoldi. Origami metamaterials for tunable thermal expansion. *Advanced Materials*, 29(26), 2017.
- [7] Jessica Burgner-Kahrs, D. Caleb Rucker, and Howie Choset. Continuum robots for medical applications: A survey. *IEEE Transactions on Robotics*, 31(6):1261–1280, 2015.
- [8] Sam Calisch. Folded functional foams. *MIT*, 2019.
- [9] David B. Camarillo, Christopher F. Milne, Christopher R. Carlson, Michael R. Zinn, and J. Kenneth Salisbury. Mechanics modeling of tendon-driven continuum manipulators. *IEEE Transactions on Robotics*, 24(6):1262–1273, 2008.
- [10] Da Chen and Xiaoyu Zheng. Multi-material Additive Manufacturing of Metamaterials with Giant, Tailorable Negative Poisson's Ratios. *Scientific Reports*, 8(1):9139, December 2018.
- [11] Kenneth C. Cheung and Neil Gershenfeld. Reversibly Assembled Cellular Composite Materials. *Science*, 341(6151):1219–1221, 2013. Publisher: American Association for the Advancement of Science _eprint: <https://science.sciencemag.org/content/341/6151/1219.full.pdf>.

- [12] Ignazio Dimino, Giovanni Andreutti, Frédéric Moens, Federico Fonte, Rosario Pecora, and Antonio Concilio. Integrated design of a morphing winglet for active load control and alleviation of turboprop regional aircraft. *Applied Sciences*, 11(5), 2021.
- [13] Kevin C. Galloway, Kaitlyn P. Becker, Brennan Phillips, Jordan Kirby, Stephen Licht, Dan Tchernov, Robert J. Wood, and David F. Gruber. Soft robotic grippers for biological sampling on deep reefs. *Soft Robotics*, 3(1):23–33, 2016. PMID: 27625917.
- [14] Lorna J. Gibson and Michael F. Ashby. *Cellular Solids: Structure and Properties*. Cambridge Solid State Science Series. Cambridge University Press, 2 edition, 1997.
- [15] J. Ginepro and Thomas C. Hull. Counting miura-ori foldings. *J. Integer Seq.*, 17:14.10.8, 2014.
- [16] James Groves Glen Bull. The democratization of production. (*International Society for Technology in Education*, pages 36–38, 2009.
- [17] I.A. Gravagne, C.D. Rahn, and I.D. Walker. Large deflection dynamics and control for planar continuum robots. *IEEE/ASME Transactions on Mechatronics*, 8(2):299–307, 2003.
- [18] I.A. Gravagne and I.D. Walker. On the kinematics of remotely-actuated continuum robots. In *Proceedings 2000 ICRA. Millennium Conference. IEEE International Conference on Robotics and Automation. Symposia Proceedings (Cat. No.00CH37065)*, volume 3, pages 2544–2550 vol.3, 2000.
- [19] Christine E. Gregg, Joseph H. Kim, and Kenneth C. Cheung. Ultra-light and scalable composite lattice materials. *Advanced Engineering Materials*, 20(9):1800213, 2018.
- [20] Elliot W. Hawkes, Laura H. Blumenschein, Joseph D. Greer, and Allison M. Okamura. A soft robot that navigates its environment through growth. *Science Robotics*, 2(8), 2017. Publisher: Science Robotics _eprint: <https://robotics.sciencemag.org/content/2/8/eaan3028.full.pdf>.
- [21] Benjamin Jenett, Christopher Cameron, Filippos Tournomousis, Alfonso Parra Rubio, Megan Ochalek, and Neil Gershenfeld. Discretely assembled mechanical metamaterials. *Science Advances*, 6(47), 2020.
- [22] Liqiao Jing, Zuoqia Wang, Bin Zheng, Huaping Wang, Yihao Yang, Lian Shen, Wenyan Yin, Erping Li, and Hongsheng Chen. Kirigami metamaterials for reconfigurable toroidal circular dichroism. *NPG Asia Materials*, 10(9):888–898, September 2018.
- [23] B.A. Jones and I.D. Walker. Kinematics for multisection continuum robots. *IEEE Transactions on Robotics*, 22(1):43–55, 2006.

- [24] Song Sang-Eun Hata N Kato T, Okumura Ichiro. Tendon-driven continuum robot for endoscopic surgery: Preclinical development and validation of a tension propagation model. 2015.
- [25] Praveen Kumar, Tanweer Ali, and M. M. Manohara Pai. Electromagnetic metamaterials: A new paradigm of antenna design. *IEEE Access*, 9:18722–18751, 2021.
- [26] George V. Lauder and Eric D. Tytell. Hydrodynamics of Undulatory Propulsion. In *Fish Physiology*, volume 23, pages 425–468. Elsevier, 2005.
- [27] Hongshuai Lei, Chuanlei Li, Xiaoyu Zhang, Panding Wang, Hao Zhou, Zeang Zhao, and Daining Fang. Deformation behavior of heterogeneous multi-morphology lattice core hybrid structures. *Additive Manufacturing*, 37:101674, 2021.
- [28] Shuguang Li, Samer A. Awale, Katharine E. Bacher, Thomas J. Buchner, Cosimo Della Santina, Robert J. Wood, and Daniela Rus. Scaling up soft robotics: A meter-scale, modular, and reconfigurable soft robotic system. *Soft Robotics*, 0(0):null, 0. PMID: 33769081.
- [29] Huai-Ti Lin, Gary G Leisk, and Barry Trimmer. GoQBot: a caterpillar-inspired soft-bodied rolling robot. *Bioinspiration & Biomimetics*, 6(2):026007, June 2011.
- [30] Jonathan A Lovegren and R John Hansman. Quantification of Fuel Burn Reduction in Cruise Via Speed and Altitude Optimization Strategies. page 97.
- [31] McNeel. “grasshopper - generative modeling for rhino. <http://grasshopper.rhino3d.com/>.
- [32] Sang Soon Oh and Ortwin Hess. Chiral metamaterials: enhancement and control of optical activity and circular dichroism. *Nano Convergence*, 2(1):24, November 2015.
- [33] Cagdas D. Onal and Daniela Rus. A modular approach to soft robots. pages 1038–1045, 2012.
- [34] C. Preisinger. “karamba, linking structure and parametric geometry”. *Archit Design*, 2013.
- [35] Priyanka Rao, Quentin Peyron, Sven Lilge, and Jessica Burgner-Kahrs. How to model tendon-driven continuum robots and benchmark modelling performance. *Frontiers in Robotics and AI*, 7:223, 2021.
- [36] Priyanka Rao, Quentin Peyron, Sven Lilge, and Jessica Burgner-Kahrs. How to model tendon-driven continuum robots and benchmark modelling performance. *Frontiers in Robotics and AI*, 7, 02 2021.

- [37] Edwar J. Roach. The wright company, from invention to industry. <https://www.jstor.org/stable/j.ctt5vjsh9>.
- [38] Matthias Rolf and Jochen J. Steil. Constant curvature continuum kinematics as fast approximate model for the bionic handling assistant. In *2012 IEEE/RSJ International Conference on Intelligent Robots and Systems*, pages 3440–3446, 2012.
- [39] Kazuya Saito, Sergio Pellegrino, and Taketoshi Nojima. Manufacture of arbitrary cross-section composite honeycomb cores based on origami techniques. volume 136, 08 2013.
- [40] Tobias A. Schaedler and William B. Carter. Architected cellular materials. *Annual Review of Materials Research*, 46(1):187–210, 2016.
- [41] Mark Schenk and Simon D. Guest. Geometry of miura-folded metamaterials. *Proceedings of the National Academy of Sciences*, 110(9):3276–3281, 2013.
- [42] R. F. Shepherd, F. Ilievski, W. Choi, S. A. Morin, A. A. Stokes, A. D. Mazzeo, X. Chen, M. Wang, and G. M. Whitesides. Multigait soft robot. *Proceedings of the National Academy of Sciences*, 108(51):20400–20403, December 2011.
- [43] Michael Sinapius, Hans Peter Monner, Markus Kintscher, and Johannes Riemschneider. Dlr’s morphing wing activities within the european network. *Procedia IUTAM*, 10:416–426, 2014. Mechanics for the World: Proceedings of the 23rd International Congress of Theoretical and Applied Mechanics, ICTAM2012.
- [44] Clean Sky. The rationale behind clean sky’s ’morphing wing for regional aircraft. 1997.
- [45] E.A. Starke and J.T. Staley. Application of modern aluminum alloys to aircraft. *Progress in Aerospace Sciences*, 32(2):131–172, 1996.
- [46] Tomohiro Tachi. Freeform rigid-foldable structure using bidirectionally flat-foldable planar quadrilateral mesh. In Cristiano Ceccato, Lars Hesselgren, Mark Pauly, Helmut Pottmann, and Johannes Wallner, editors, *Advances in Architectural Geometry 2010*, pages 87–102, Vienna, 2010. Springer Vienna.
- [47] M. S. Triantafyllou, A. H. Techet, Q. Zhu, D. N. Beal, F. S. Hover, and D. K. P. Yue. Vorticity Control in Fish-like Propulsion and Maneuvering1. *Integrative and Comparative Biology*, 42(5):1026–1031, November 2002.
_eprint: <https://academic.oup.com/icb/article-pdf/42/5/1026/1877903/i1540-7063-042-05-1026.pdf>.
- [48] Michael S. Triantafyllou and George S. Triantafyllou. An Efficient Swimming Machine. *Scientific American*, 272(3):64–70, March 1995.

- [49] Michael Wehner, Ryan L. Truby, Daniel J. Fitzgerald, Bobak Mosadegh, George M. Whitesides, Jennifer A. Lewis, and Robert J. Wood. An integrated design and fabrication strategy for entirely soft, autonomous robots. *Nature*, 536(7617):451–455, 2016.